NREL/TP-413-4906 • UC Category: 273 • DE92010584

NREL/TP--413-4906

DE92 010584

Research on Polycrystalline Thin Film Submodules Based on $CuInSe_2$ Materials

Annual Subcontract Report
11 November 1990 - 31 October 1991

A. Catalano, R. Arya, L. Carr,
B. Fieselmann, T. Lommasson,
R. Podlesny, L. Russell, S. Skibo,
A. Rothwarf, R. Birkmire
Solarex Corporation
Newtown, Pennsylvania

NREL technical monitor: H.S. Ullal

National Renewable Energy Laboratory
1617 Cole Boulevard
Golden, Colorado 80401-3393
A Division of Midwest Research Institute
Operated for the U.S. Department of Energy
under Contract No. DE-AC02-83CH10093

Prepared under Subcontract No. ZN-1-19019-4

May 1992

On September 16, 1991 the Solar Energy Institute was designated a national laboratory, and its name was changed to the National Renewable Energy Laboratory.

Printed in the United States of America
Available from:
National Technical Information Service
U.S. Department of Commerce
5285 Port Royal Road
Springfield, VA 22161

Price: Microfiche A01
Printed Copy A05

Codes are used for pricing all publications. The code is determined by the number of pages in the publication. Information pertaining to the pricing codes can be found in the current issue of the following publications which are generally available in most libraries: *Energy Research Abstracts (ERA)*; *Government Reports Announcements* and Index (*GRA* and I); *Scientific and Technical Abstract Reports (STAR)*; and publication NTIS-PR-360 available from NTIS at the above address.

EXECUTIVE SUMMARY

Objectives: The principal objective of this three-year research program is to develop 12% efficient CIS submodules with area > 900 cm^2. To meet this objective the program is divided into five tasks: (1) Windows, Contacts, Substrates, (2) Absorber Material, (3) Device Structure, (4) Submodule Design and Encapsulation and (5) Process Optimization. In the first year of the program, efforts were concentrated on the first three tasks with an objective to demonstrate a 9% efficient CIS solar cell.

Task I: Windows, Contacts, Substrates

The window layer under development consists of two films, cadmium sulphide (CdS) and Zinc Oxide (ZnO). The CdS thin film is deposited by chemical solution growth from a mixture of $CdCl_2$, NH_4Cl, NaOH and Thiourea. At low temperature (< 90°C), the self-limiting reaction deposits approximately 1200Å thick CdS film on glass substrates. The films are stoichiometric and highly uniform over 3" x 3" substrates. The dark conductivity is high, in the range of 10^8 to 10^9 Ω-cm. Films with thicknesses varying from 500Å to 1 μm have been deposited, the thicker films being deposited by successive depositions. The transmission of light for wavelengths below the CdS cut-off (~ 500 nm) occurs for film thicknesses less than approximately 4000Å. For example, the transmission of light at 400 nm is about 20% and 40% for about 1000Å and about 500Å thick CdS films, respectively. CdZnS films have also been deposited by the same process. These films show an increase in bandgap as demonstrated by a shift in the transmission towards shorter wavelengths.

A process has been developed to deposit ZnO films by low-pressure chemical vapor deposition (LPCVD). The deposition is carried out at low temperatures (< 200°C) with feedstock of diethylzinc (DEZ), water and diborane gas. The two main properties required in a good window layer - high optical transmission (in the wavelength range of 400 nm - 1400 nm) and high electrical conductivity (< 10 Ω/□) are interdependent. The transmission of ZnO films, particularly at long wavelengths (> 1000 nm) is found to be a strong function of the dopant gas concentration and film thickness. It decreases rapidly as the dopant concentration or the thickness is increased. The conductivity, on the other hand, increases with an increase in dopant concentration and film thickness at a given deposition temperature. Hence, a compromise has to be made

Two major problems have been encountered in the deposition of CIS films by sputtering from elemental targets. Both these problems are related to sputtering of Se. Due to the low thermal conductivity of Se, hotspots can develop in the Se target which result in non-uniform sputtering. Non-uniform sputtering perturbs the spatial and temporal uniformity of the Se flux. Furthermore, due to the proximity of the targets in our deposition system, the Cu- and In- targets are contaminated by the Se flux. The selenide layers that form on top of the Cu- and In- targets can reduce the specific Cu and In flux by as much as 50% and 20%, respectively. This had led to poor run-to-run reproducibility. Nevertheless, CIS films with good composition have been deposited. Two approaches are underway to overcome this problem. First, Cu and In films have been sputtered and the stack selenized in a Se vapor with an inert carrier gas in a tube furnace at temperatures between 400°C - 450°C. This has resulted in films in which the composition was Cu = 22.8%, In = 23.7%, and Se = 53.5%. Second, the Se target has been replaced by a resistive heated evaporation source. This hybrid arrangement of sputtered Cu and In and evaporated Se has successfully solved the problem of target cross-contamination. Good CIS film composition has been achieved with this process but the surface morphology of the films are still poor. Both these approaches are at an early stage of development.

Task III: Device Structure

Solar cells have been fabricated with two device structures:

(i) Light => Ni-Al grid / ZnO / thin CdS / CIS / Mo / Glass
(ii) Light => Ni-Al grid / ITO / thick CdS / CIS / Mo / Glass

The device structure (i) has been employed with all layers deposited at Solarex, whereas the device structure (ii) has been employed by IEC on CIS deposited at Solarex. Several devices with either device structure have resulted in conversion efficiencies above 5%. The best device fabricated on sputtered CIS had a conversion efficiency of 6.2% with the following photovoltaic parameters: $V_{oc} = 0.343V$, $J_{sc} = 31.9\ mA/cm^2$ and FF = 0.562. The best device fabricated on hybrid CIS films had a conversion efficiency also of 6.2% but with the following photovoltaic parameters: $V_{oc} = 0.373V$, $J_{sc} = 35.5\ mA/cm^2$ and FF = 0.474. The poor V_{oc} is attributed to the surface morphology of the CIS films. A quantum efficiency apparatus has been designed and assembled which can measure QE's from 400 nm to 1400 nm.

(3) To assess future designs using compositions other than CIS, i.e. $CuIn_{1-x}Ga_xSe_{2(1-y)}S_{2y}$, etc., we have considered whether varying the conduction band and/or the valence band will be more effective in increasing the efficiency of the cell. Both analytic modeling and numerical simulation have been started. Initial analysis suggests that it is the valence band that should be varied. Fundamental calculations of the band edges in compound semiconductors have not yet been carried out for the substitution of S for Se rather than Ga for In is more likely to move the valence band of CIS down. How that variation should be used in a graded bandgap region has not yet been established. An analytic expression for the dark diode current of an insulating graded bandgap solar cell has been obtained, for the case of the gap increasing linearly away from the junction. The results indicate a diode factor ranging from - 1.6 at low voltages to 2 at higher voltages. An increase in open-circuit voltage is expected to be roughly half of the increase in the energy gap, subject, however, to a maximum value set by the smaller of the built-in voltages in the conduction or valence bands. The numerical simulator is being used to explore the I-V curves for various grading profiles.

Institute of Energy Conversion (IEC)

IEC personnel have strongly contributed to all three tasks of this program. In Task I, we have interacted in the development of CdS thin films by the chemical solution growth method. The deposition system was set-up at Solarex after consultations with IEC personnel. IEC was also involved in the initial development of process parameters and film characterization. In Task II, IEC has contributed in three major areas. First, they have supplied us with an ample number of CIS films deposited on Mo to evaluate our window layers. Second, they have characterized our CIS material by X-ray diffraction, SEM microscopy, EDX analysis and Atomic Absorption measurements. Third, they have supported this program as technical consultants in the process development of CIS by sputtering and sputtering/evaporation.

In Task III, IEC has fabricated and characterized solar cells on Solarex deposited CIS material. These cells were fabricated with evaporated CdS heterojunctions and resulted in the highest conversion efficiency (6.2%) that we achieved on sputtered CIS material.

TABLE OF CONTENTS

Section Page

LIST OF FIGURES

LIST OF FIGURES (continued)

LIST OF FIGURES (continued)

LIST OF TABLES

1.0 INTRODUCTION

Copper indium diselenide ($CuInSe_2$), also known as CIS, has emerged as an important photovoltaic material for low-cost, thin film solar cells and submodules. Several organizations (1,2,3) have reported high conversion efficiencies (> 12%) with the highest being 14.1% (4). CIS modules have been scaled-up to 1 square foot and 4 square foot sizes. Conversion efficiencies > 10% have been reported for these large area modules (5).

All high efficiency CIS solar cells and submodules reported to date have been prepared by either of the two methods - (i) simultaneous co-evaporation of the three elements Cu, In and Se onto substrates held at elevated temperatures or (ii) a two-stage process in which the Cu and In metal layers are deposited either by evaporation or sputtering and then this stack is selenized in an H_2Se ambient at temperatures between 400°C - 450°C (5,6).

The first method is not amenable to large area scale-up and hence is not being pursued for terrestrial applications. Even though the second method is the only method of preparing CIS that has been successfully scaled-up to large areas, it has two limitations - (i) it requires selenization in toxic H_2Se gas to form the CIS compound, and (ii) since the selenization of Cu/In stacks results in approximately a three-fold volume expansion, it is believed to result in poor adhesion at the Mo/CIS interface (7).

A method to prepare CIS which overcomes these two limitations would be far preferable for large area terrestrial applications.

In our research program, we have been addressing all the key elements of CIS solar cells. We have developed the window layers which consists of CdS thin films deposited by chemical solution growth and ZnO thin films deposited by low pressure chemical vapor deposition (LPCVD). We have chosen to deposit CIS by sputtering from elemental targets onto substrates held at elevated temperatures. This method is similar to the three-source evaporation method in that the flux of species that arrive at the substrate are elemental and the compound formation takes place on the heated substrate. However, sputtering offers several advantages over the evaporation method. Sputtered films can be deposited over large areas with ease and with excellent control over spatial uniformity.

Problems associated with sputtering of Se have led us to replace the sputtered Se with evaporation of Se from a thermally heated source. CIS solar cells have been fabricated by employing either a thick CdS window layer (done at IEC) or by depositing a thin CdS and ZnO layer.

2.0 TASK I: WINDOWS, CONTACTS, SUBSTRATES

2.1 Windows

The window layer under development consists of two thin films, cadmium sulphide (CdS) and zinc oxide (ZnO). The deposition of CdS films is carried out by the solution growth method and the deposition of ZnO is carried out by low pressure chemical vapor deposition (LPCVD). The selection of these processes were made with low cost manufacturability and large area scale-up compatibility considerations.

2.1.1 CdS Film Deposition Process

CdS thin films have been deposited by chemical solution growth from a mixture of $CdCl_2$, NH_4Cl, NaOH and Thiourea. A schematic diagram of the apparatus is shown in **Figure 2-1**. In this process the chemical reaction of $CdCl_2$ provides the Cd^{++} ions, Thiourea provides the S^{--} ions, ammonia acts as a complexing agent and NH_4Cl acts as a buffer. The chemical reactions that take place are:

Decomposition of Thiourea:

$$(NH_2)\,C\,S + OH^- \Rightarrow CH_2N_2 + H_2O = HS^-$$
$$HS^- = OH^- \Rightarrow S^{--} + H_2O$$

Cadmium Sulphide Formation:

$$Cd^{++} + 4\,NH_3 \Rightarrow Cd\,(NH_3)_4{}^{++}$$
$$Cd(NH_3)_4{}^{++} + S^{--} \Rightarrow CdS + 4\,NH_3$$

The rate of CdS film formation is strongly dependent on the concentrations of Cd^{++}, S^{--} ions, bath temperature and pH of the solution. At low temperatures (< 90°C), the self-limiting reaction deposits approximately 1200Å thick CdS film on glass substrates. CdZnS thin films have been deposited by the addition of $ZnCl_2$ to the solution.

2.1.2 CdS Film Characterization

We have studied the CdS films for their spatial uniformity, compositional, electrical and optical properties.

Figure 2-1. Schematic diagram of apparatus for chemical deposition of CdS.

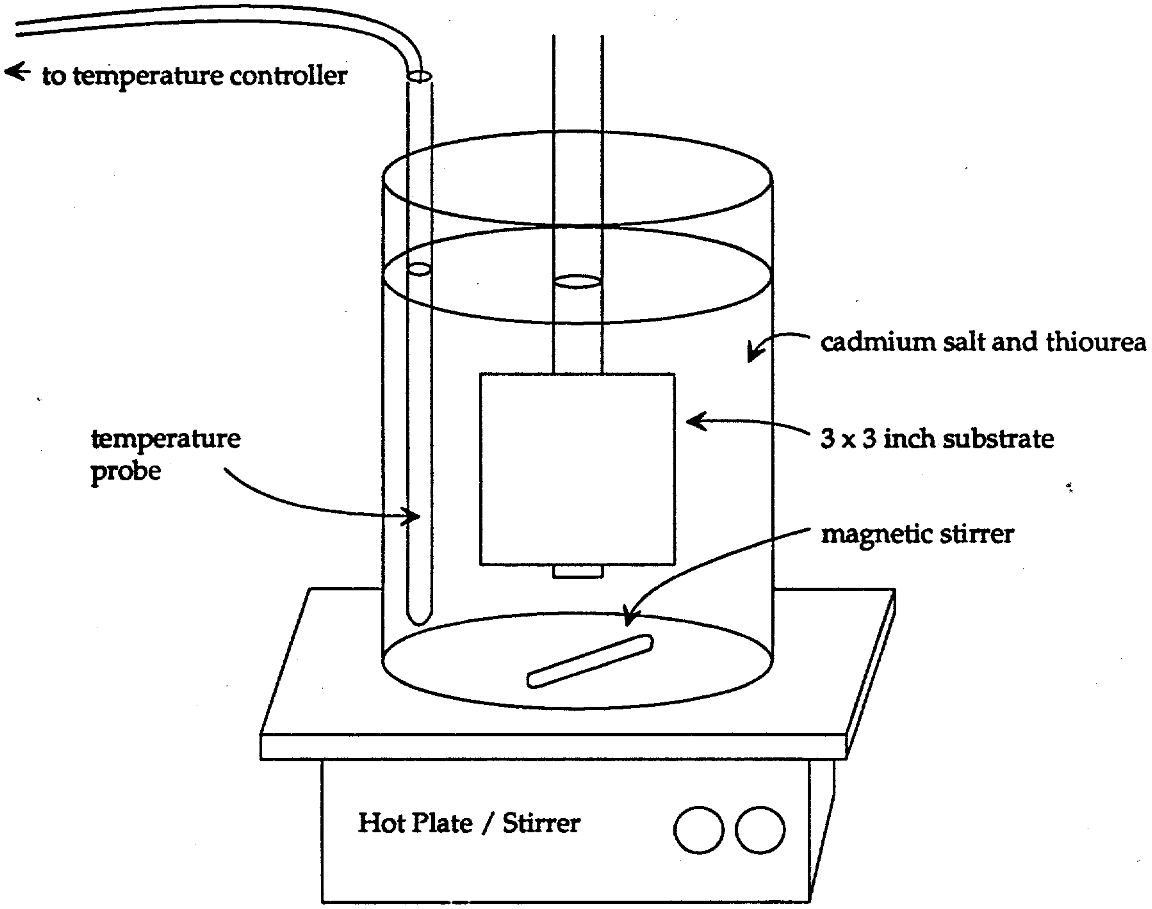

CdS films deposited on glass or tin oxide coated glass substrates exhibit excellent spatial uniformity over 3" x 3" substrates. **Figure 2-2** shows the spatial uniformity of transmission versus wavelength of a 1700Å thick CdS film (Sample # 1-007A). The 3" x 3" substrate was divided into a matrix of nine 1" x 1" samples. The measurements are shown for five locations (the four corners and the middle of the 3" x 3" sample). **Figure 2-3** shows similar measurements made on a 1350Å thick CdZnS film.

CdS films have been deposited with thicknesses varying from 500Å to 1 μm, the thicker films were deposited by successive depositions. **Figure 2-4** shows the transmission of CdS films as a function of film thickness. The transmission of light for wavelengths below the CdS cut-off (~ 500 nm) occurs for film thicknesses less than approximately 4000Å.

Energy dispersive X-ray analysis (EDX) measurements of CdS films indicate that they are nearly stoichiometric. Lateral dark conductivity measurements show that these films have conductivity in the range of 10^{-8} - 10^{-10} $(\Omega\text{-cm})^{-1}$. The electrical conductivities of some typical CdS films along with some CdZnS films are tabulated in **Table 2-1**. The CdZnS films are slightly less conducting than CdS films.

Table 2-1. Electrical and Optical Properties of CdS Films.

Sample #	Material	Thickness (Å)	Conductivity $(\Omega\text{-cm})^{-1}$
O270C1	CdS	1,800	3.3×10^{-10}
0270A1	CdS	2,300	1.2×10^{-8}
0268A1	CdS	4,470	4.6×10^{-9}
0253A2	CdS	10,000	2.1×10^{-8}
0253B1	CdZnS	1,880	1.2×10^{-11}
0262A1	CdZnS	4,380	8.4×10^{-10}

The formation of CdZnS was confirmed by EDX analysis. **Figure 2-5** shows the EDX spectra of a typical CdS film and a typical CdZnS film, the latter film indicating the presence of Zn. The addition of Zn to CdS widens the optical bandgap. This is clearly seen in **Figure 2-6** where the transmission versus wavelength measurements of two films of approximately equal thickness, one CdS and the other CdZnS, are plotted. The onset of transmission of the CdZnS film is shifted towards shorter wavelength indicating a wider bandgap material.

Figure 2-2. Spatial uniformity of the optical transmission of CdS film over a 3" x 3" substrate.

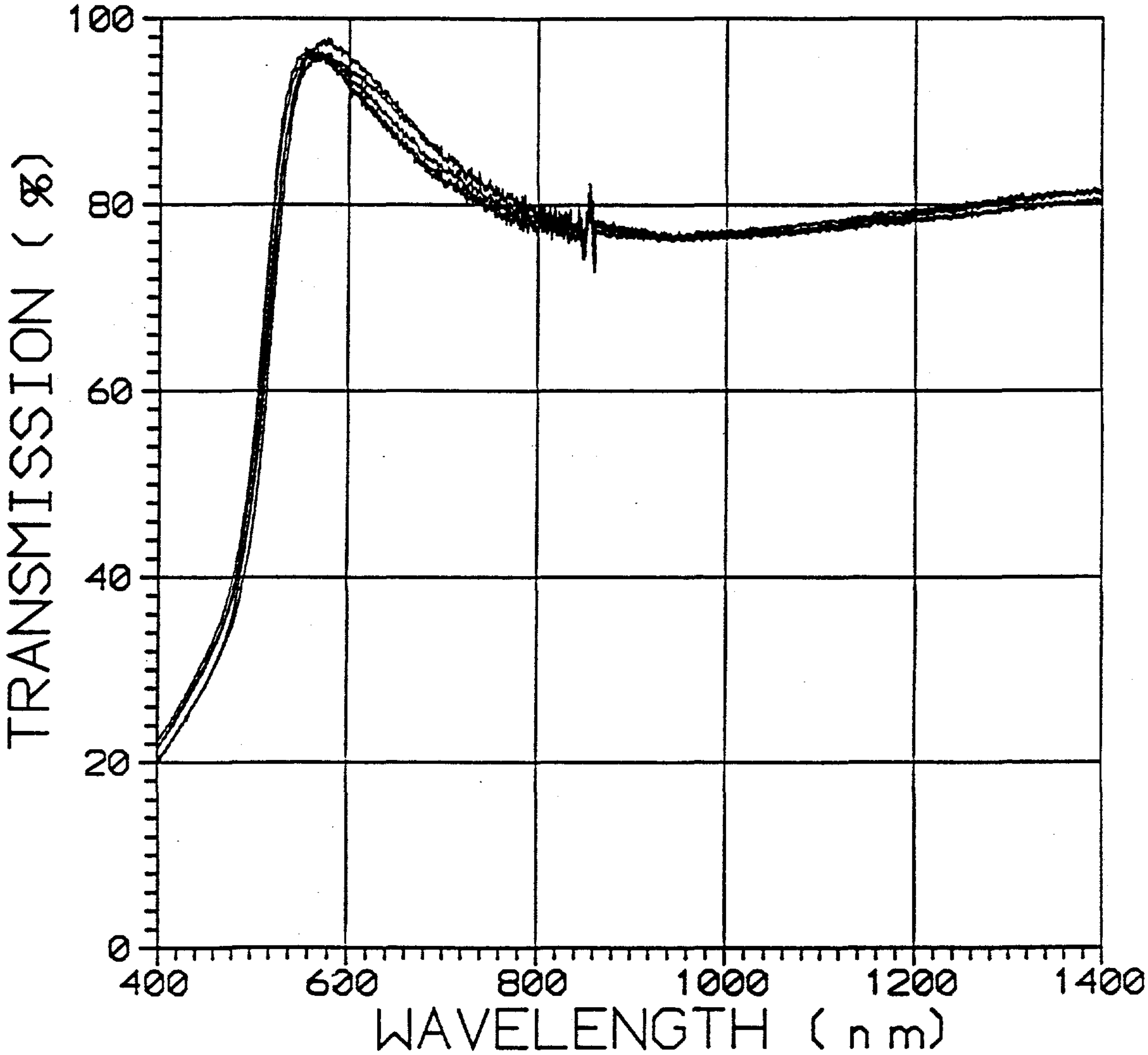

Figure 2-3. Spatial uniformity of the optical transmission of CdZnS film over a 3" x 3" substrate.

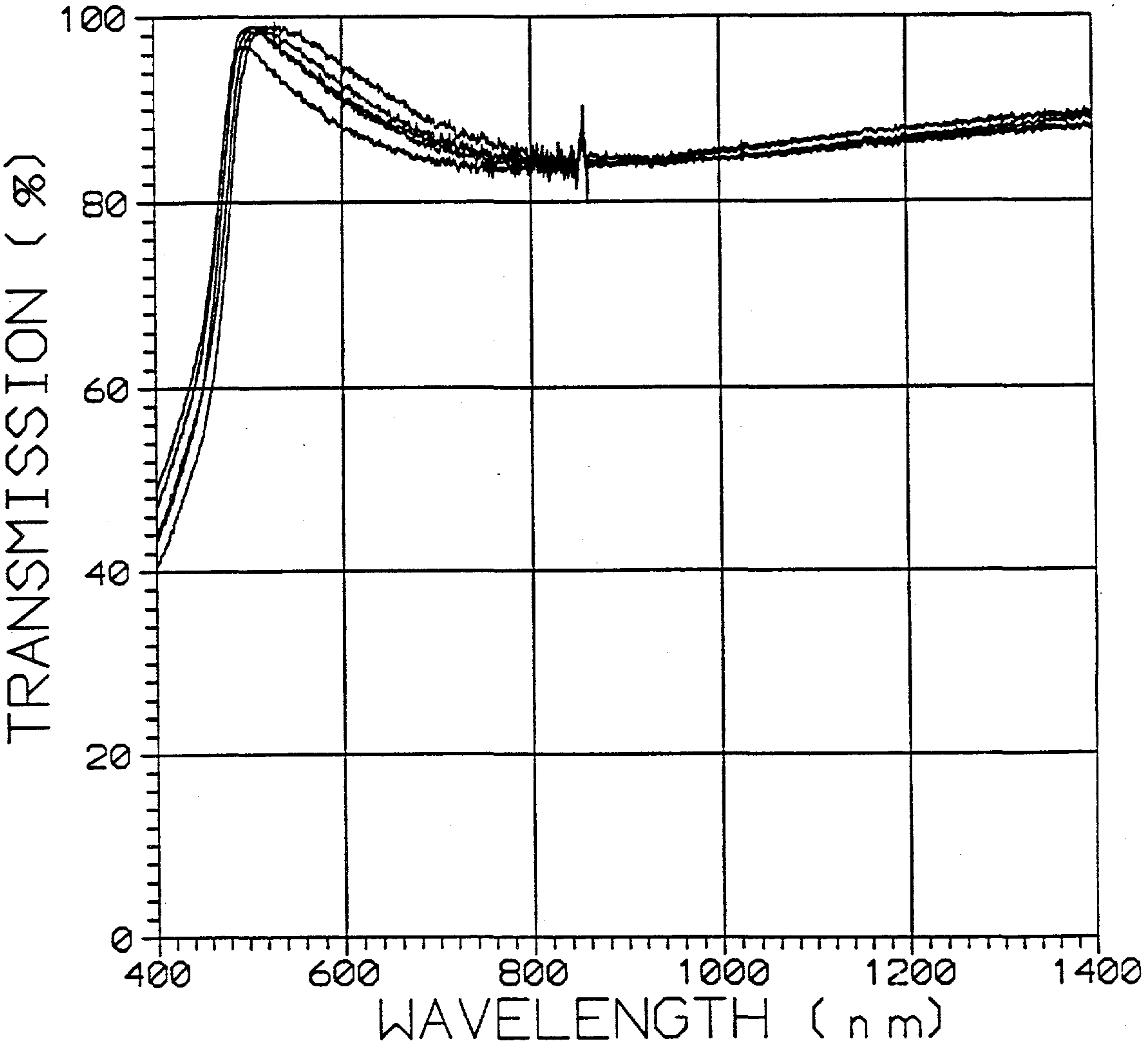

Figure 2-4. Transmission versus wavelength measurements of CdS films as a function of film thickness.

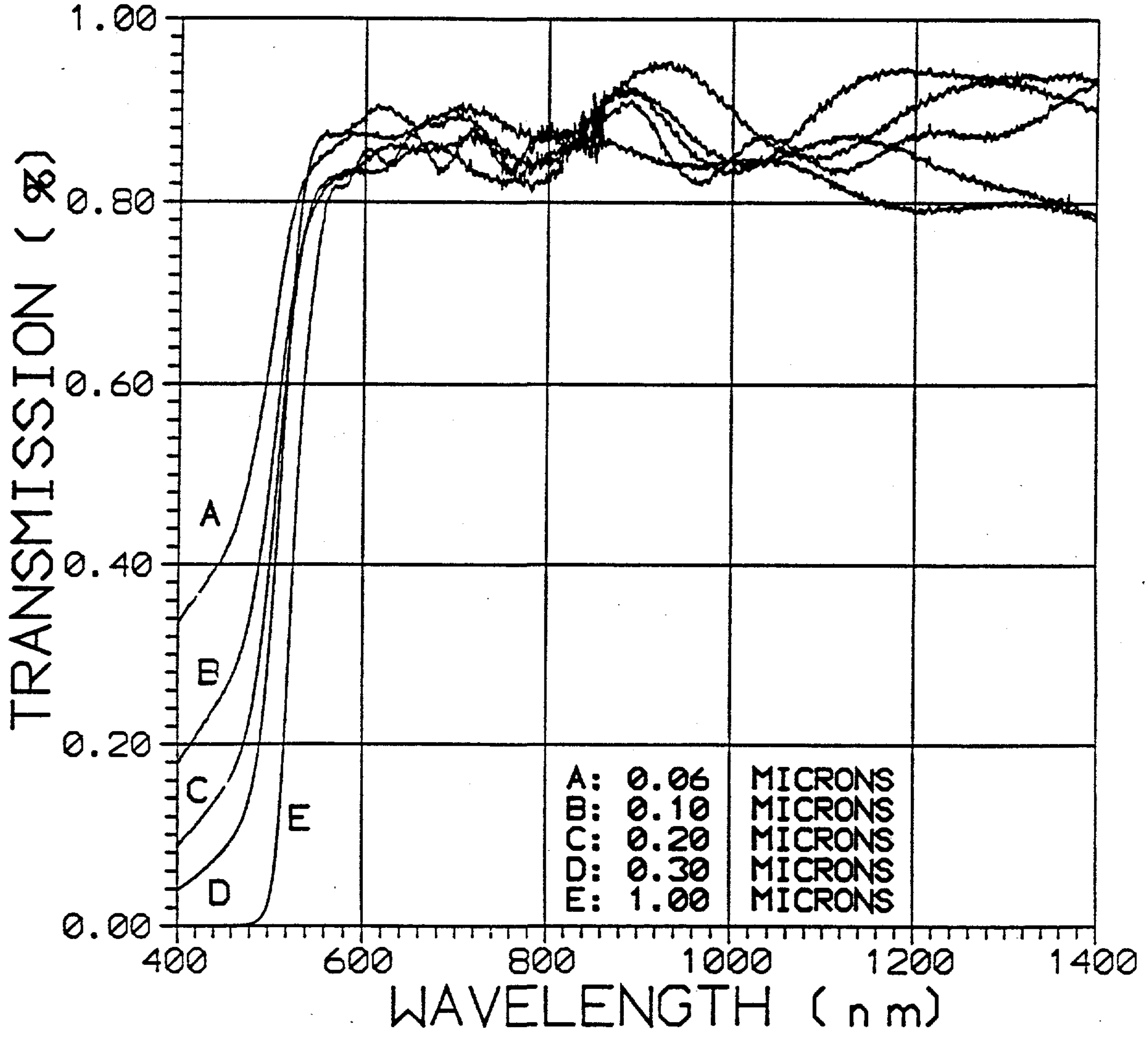

Figure 2-5. EDX spectra of CdS and CdZnS films.

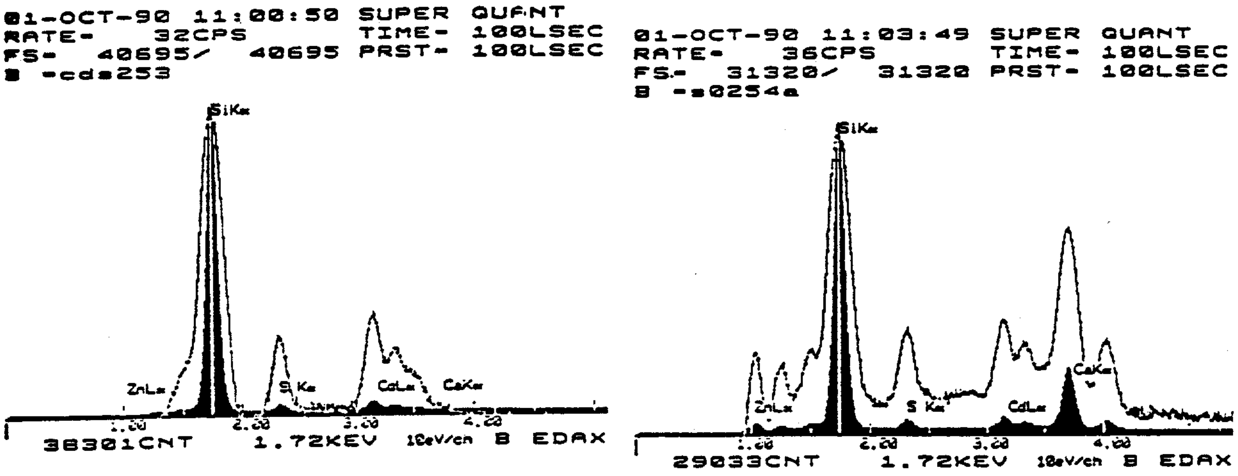

```
01-OCT-90 11:00:50 SUPER QUANT
RATE-    32CPS           TIME- 100LSEC
FS-  40695/   40695 PRST- 100LSEC
B -cds253
38301CNT      1.72KEV  10eV/ch  B  EDAX
```

```
01-OCT-90 11:03:49 SUPER QUANT
RATE-    36CPS           TIME- 100LSEC
FS-  31320/   31320 PRST- 100LSEC
B -s0254a
29033CNT      1.72KEV  10eV/ch  B  EDAX
```

CdS

CdZnS

Figure 2-6. Transmission versus wavelength measurement of CdS and CdZnS films.

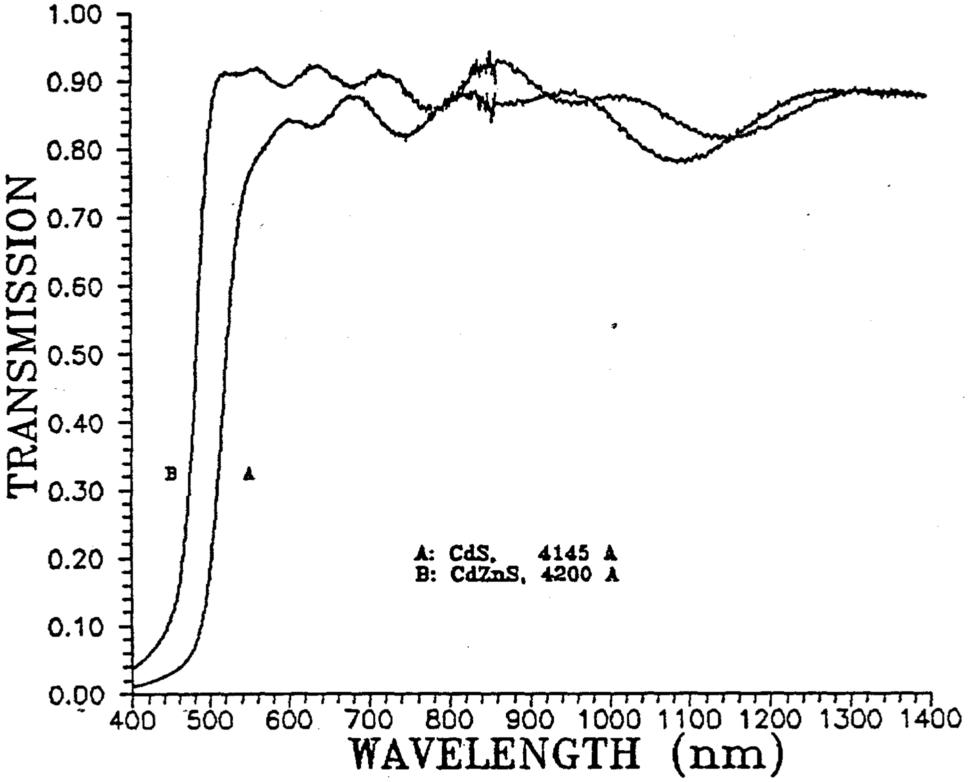

2.1.3 Zinc Oxide Deposition Process

We have developed a process to deposit zinc oxide (ZnO) thin films by low-pressure chemical vapor deposition (LPCVD). A schematic diagram of the deposition system is shown in **Figure 2-7**. The deposition is carried out at low temperatures with a feedstock of diethylzinc (DEZ), water and diborane gas. Diborane is used as the dopant gas. Typical deposition conditions are substrate temperature (150°C - 200°C), deposition pressure (1 - 5 Torr), and deposition rate (10Å - 20Å/sec.).

The two main properties required in a good window layer for CIS solar cells is high optical transmittance in the wavelength range of 400 to 1400 nm and high electrical conductivity. It is desirable to have the sheet resistance of the front contact < 10 Ω/□. These two properties are interdependent. While high optical transmission can be easily achieved in ZnO films, it is generally accompanied with high sheet resistance. Hence, a compromise has to be made between these two properties. Furthermore, often the performance of CIS solar cells is improved by post-fabrication heat-treatments in air which adds a third necessity to these films - their properties have to be stable up to several hours of heat treatments in air at ~ 200°C.

We have optimized our deposition process to address these three requirements.

2.1.4 Characterization of ZnO Films

2.1.4.1 *Electrical and Optical Properties*

We have studied the electrical properties of ZnO thin films as a function of three deposition parameters - dopant gas concentration, film thickness and deposition temperature. The sheet resistance of ZnO films is a strong function of deposition temperature in the temperature range of 160°C - 200°C, the film thickness and the dopant gas concentration. **Figure 2-8** shows the optical transmission of three ZnO films which were deposited with a constant dopant gas flow concentration and had thicknesses of about 1.5 μm but were deposited at deposition temperatures of 165°C, 188°C, and 203°C. The optical transmission, particularly the long wavelength transmission is a very strong function of deposition temperature - the films deposited at the lowest temperature being the most transparent. The sheet resistance in these films varied by a factor of two, from 5 to 10 Ω/□ - the most conducting films were deposited at the highest temperature.

The sheet resistance of ZnO films deposited at a fixed deposition temperature and fixed dopant gas flow concentrations increases as the film thickness decreases. This is shown in **Figure 2-9**

Figure 2-7. Schematic diagram of ZnO deposition system.

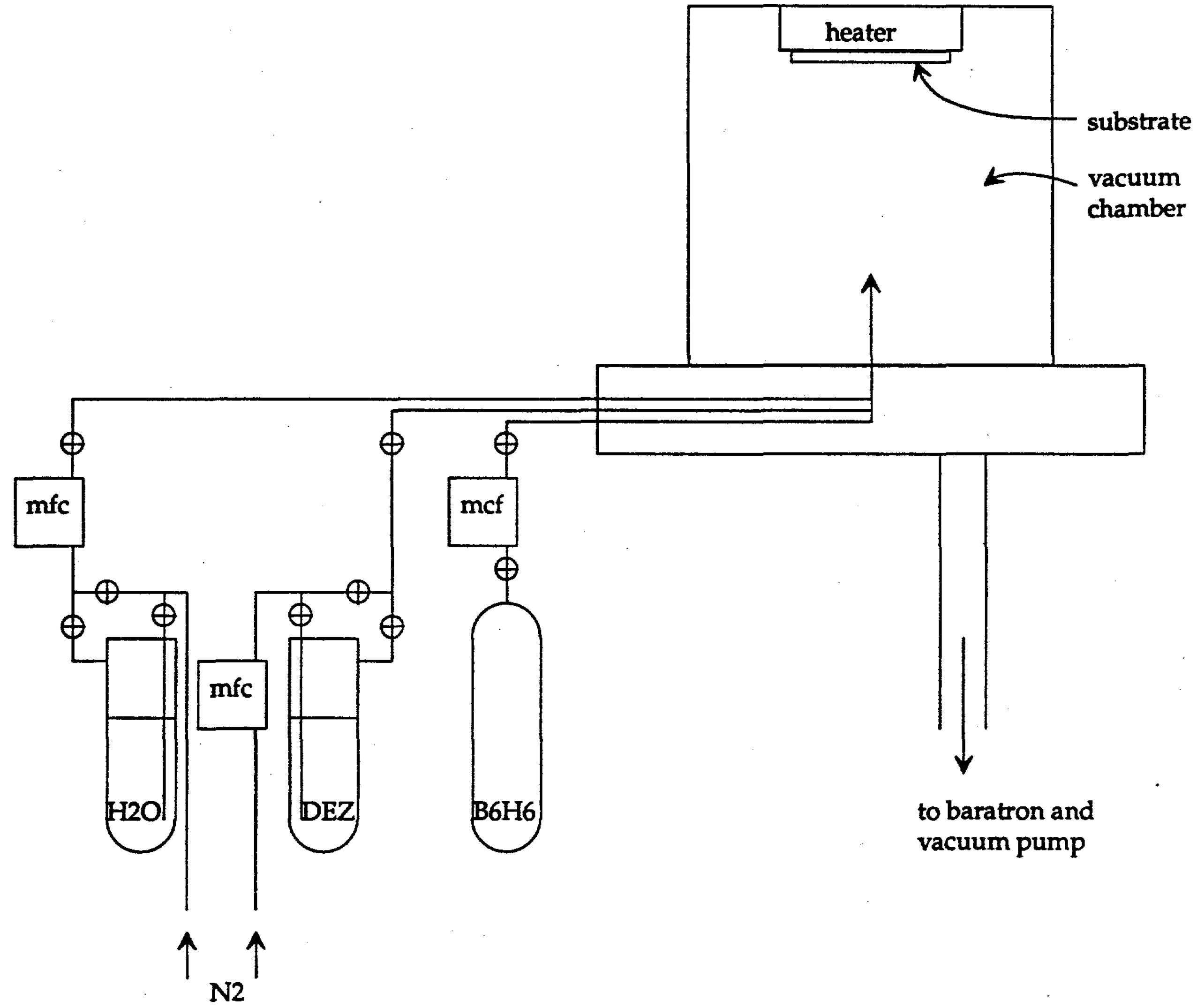

Figure 2-8. Transmission versus wavelength measurements of ZnO films as a function of deposition temperature.

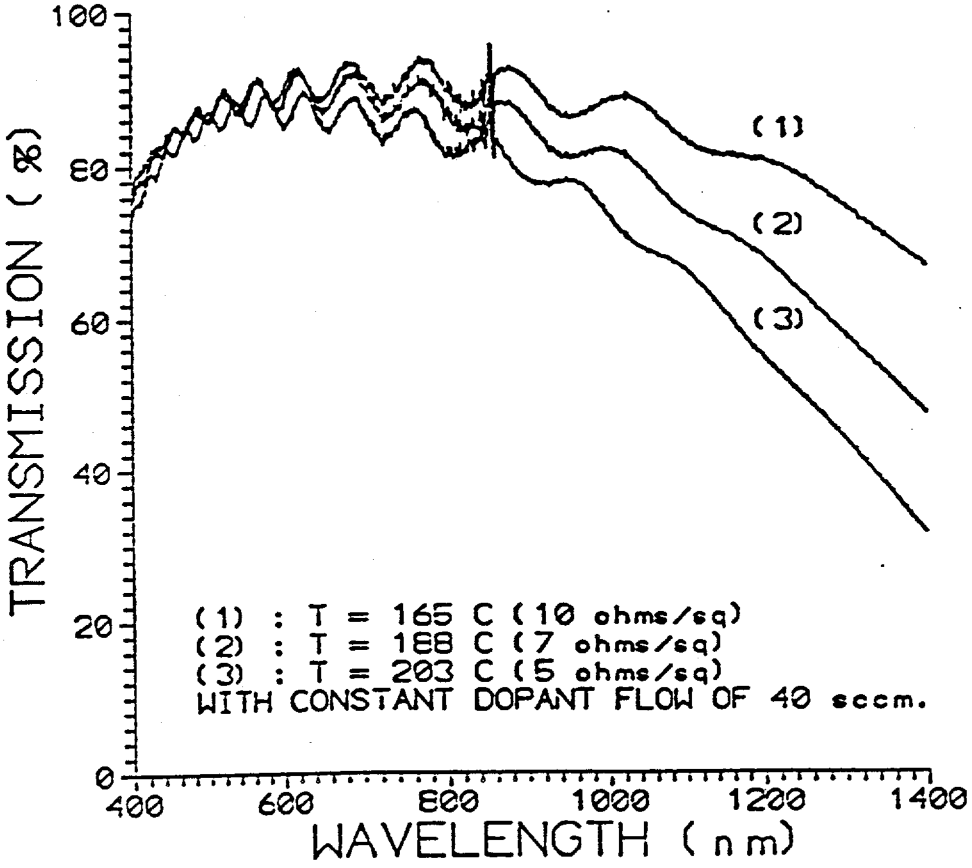

Figure 2-9. Transmission versus wavelength measurements of ZnO films as a function of film thickness.

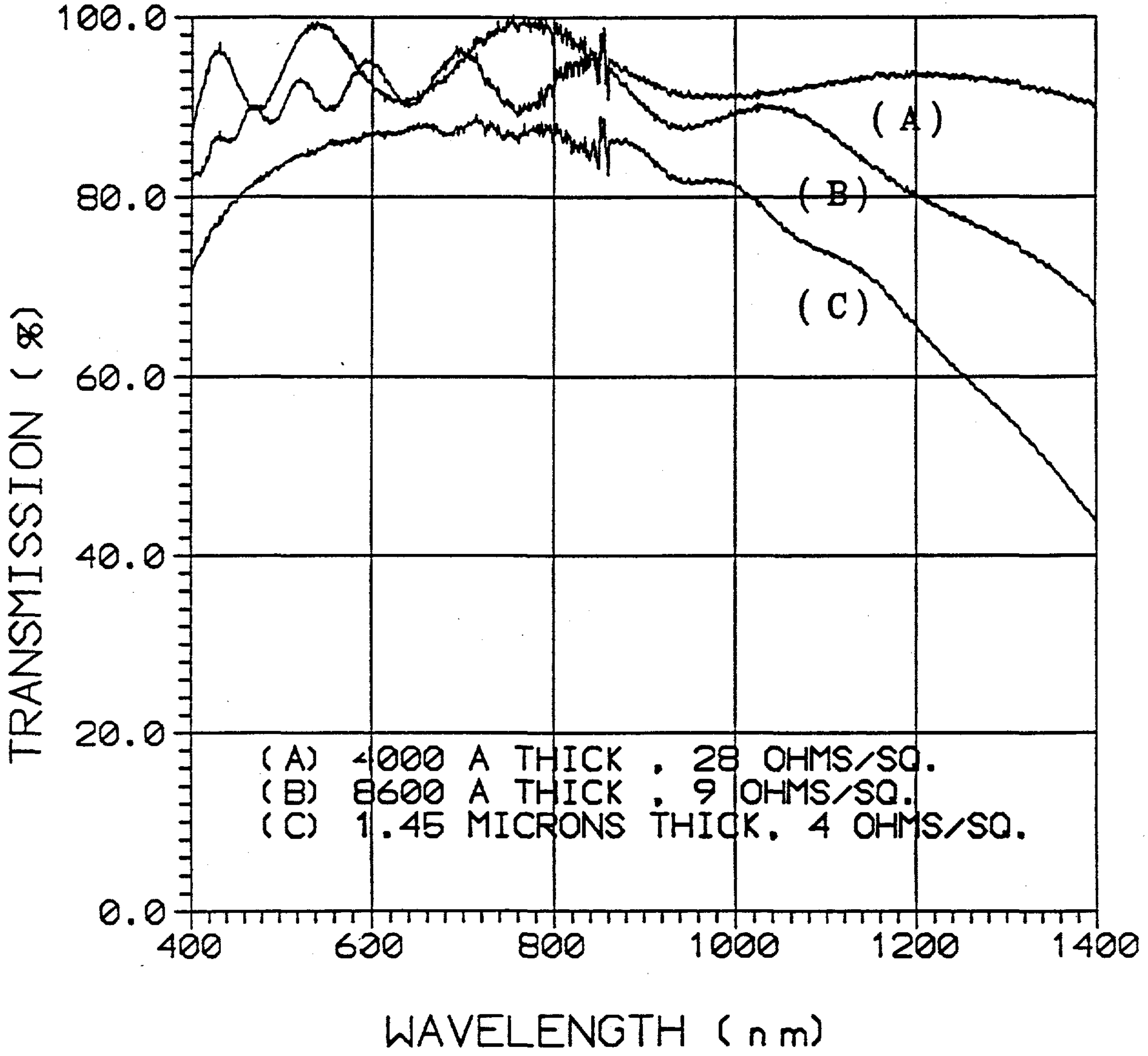

where the transmission of three ZnO films of different thicknesses are plotted. The sheet resistance increases from 4 Ω/□ to 28 Ω/□ as the film thickness decreases from 1.45 μm to 4000Å. The transmission and sheet resistance of ZnO films varies strongly with dopant gas flow concentrations at a given deposition temperature and film thickness. We have studied this effect for two different film thicknesses. **Figure 2-10** shows the transmission versus wavelength measurements of five films in which the diborane gas flow was varied from 0 to 40 sccm. These films were about 1.5 μm thick and were deposited at 180°C. Clearly, the optical transmission is strongly influenced by the dopant concentrations, particularly in the long wavelength region. The optical transmission at 1200 nm increases from approximately 65% to 95% as the dopant gas flow is decreased from 50 sccm to 0 sccm. The corresponding change in the sheet resistance increases from 7 Ω/□ to 50 Ω/□. In the second set of experiments, the film thickness was kept at 0.8 μm. **Figure 2-11** shows the transmission versus wavelength measurement of four ZnO films in which the dopant gas flow was varied from 10 sccm to 50 sccm. Once again, it was clear that the transmission in the long wavelength region was superior for the film with the least dopant gas flow. The sheet resistance of these films varied from 13 Ω/□ to 19 Ω/□. An optimum compromise was achieved in films deposited with dopant gas flow of 10 - 15 sccm. These films exhibited transmission at 1200 nm of about 90% for film thicknesses of about 1.5 μm and 95% for film thicknesses of about 0.8 μm. The corresponding sheet resistances were 9 Ω/□ and 12 Ω/□, respectively.

A study of the effect of heat treatment in air at 200°C of the films revealed that the films with the least dopant flow (10 sccm) were least stable - after one hour of heat treatment the sheet resistance increased to > 70 Ω/□, whereas the films deposited with the most dopant gas flow were the most stable. This is shown in **Figure 2-12**. These results have guided us in selecting the deposition parameters optimum for ZnO films. If we do not subject the finished devices to any post-fabrication heat treatments then a 0.8 μm thick ZnO films deposited with 10 -15 sccm dopant gas flow is optimum. On the other hand, if our devices require heat treatments, further optimization of deposition parameters are necessary.

Optimization of the window layers by reduction in CdS film thickness and ZnO film thickness and dopant gas flow has resulted in improvements in both the short wavelength and the long wavelength response of CIS devices. **Figure 2-13** shows the quantum efficiency versus wavelength measurements of two CIS cells in which the CIS was taken from the same deposition run (Run #S189). The quantum efficiency measurements were made under a reverse electrical bias of 0.25V and AM1 light bias to ensure complete collection of carriers and to properly reflect optical losses. The two devices had window layer thicknesses of: CdS = 1200Å and ZnO = 1.5 μm (Curve A) and CdS = 500Å and ZnO = 0.8 μm (Curve B), respectively. The reduction in

Figure 2-10. Transmission versus wavelength measurements of ZnO films as a function of dopant gas flow for 1.5 μm thick films.

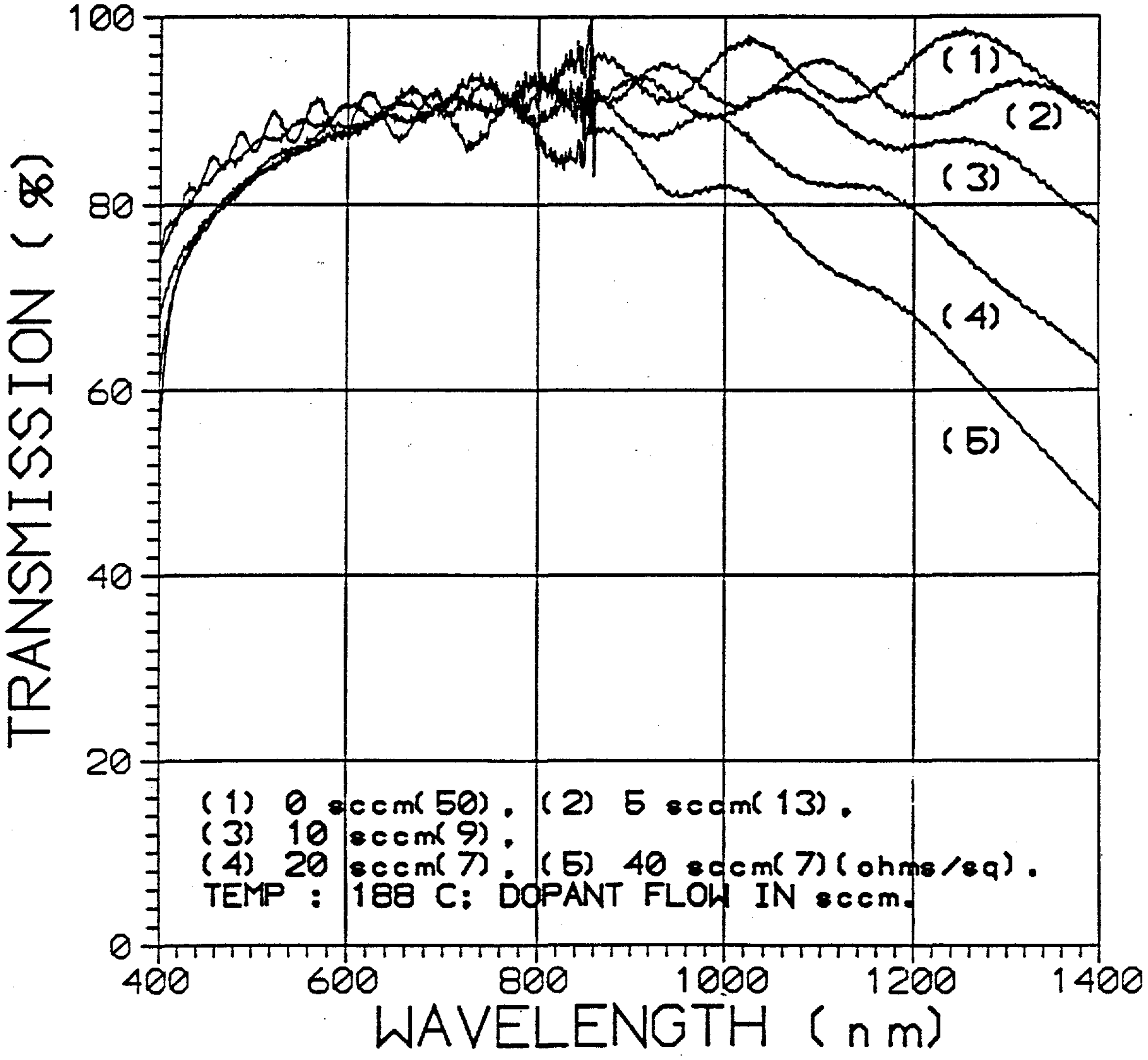

Figure 2-11. Transmission versus wavelength measurements of ZnO films as a function of dopant gas flow for 0.8 μm thick films.

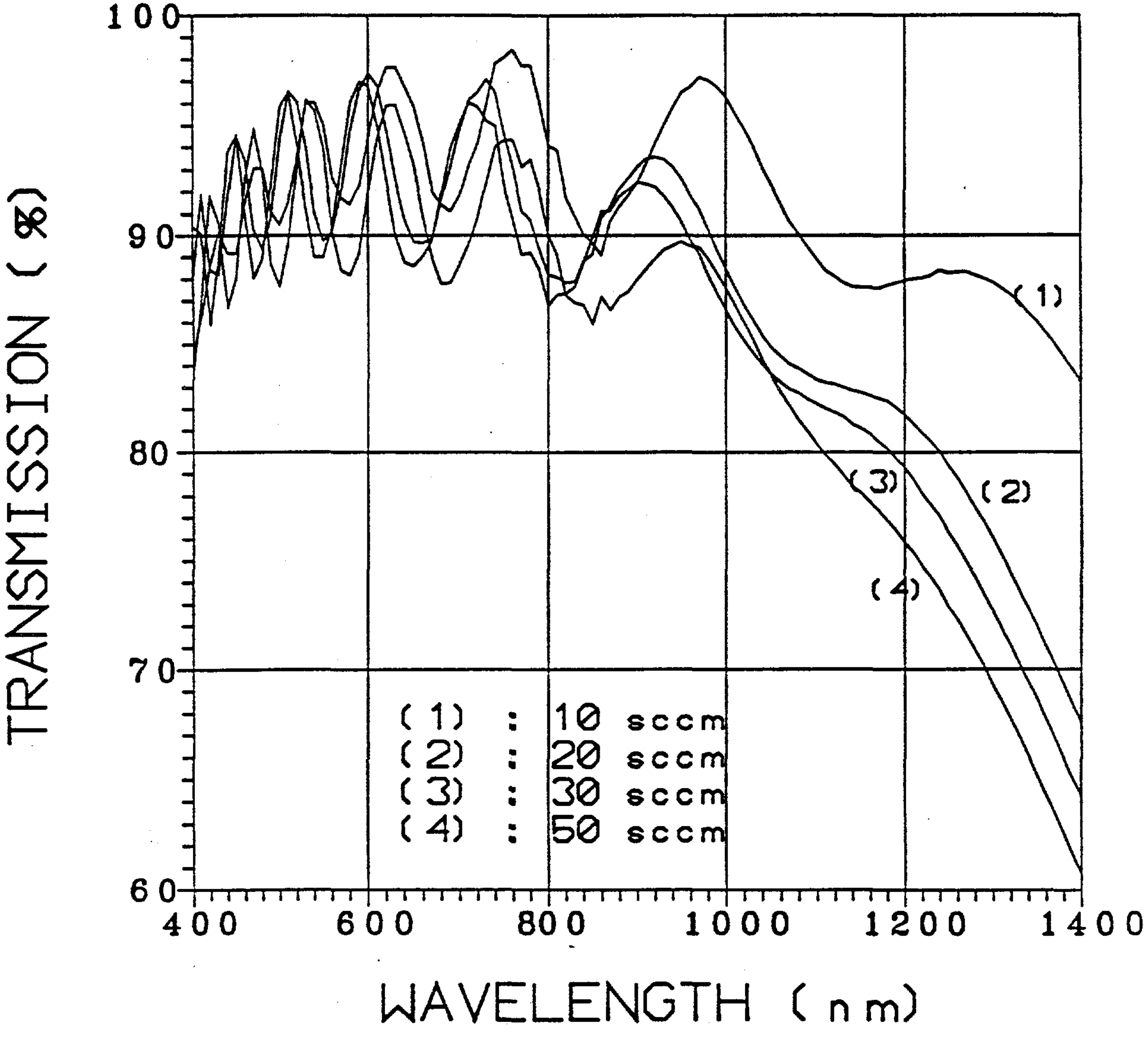

Figure 2-12. Effect of heat-treatment on sheet resistance of ZnO films shown in **Figure 2-11.**

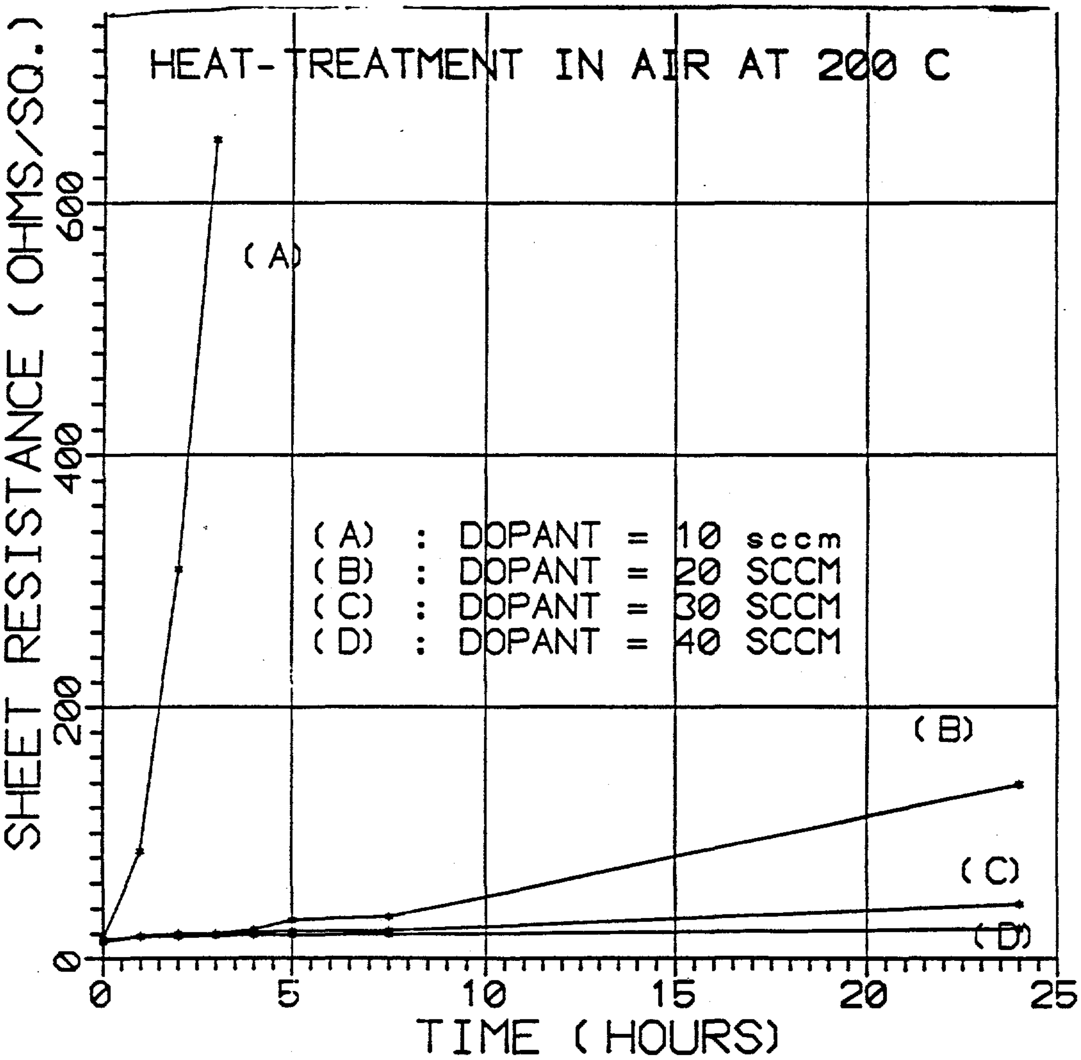

Figure 2-13. Effect of window layers on the quantum efficiency of CIS solar cells.

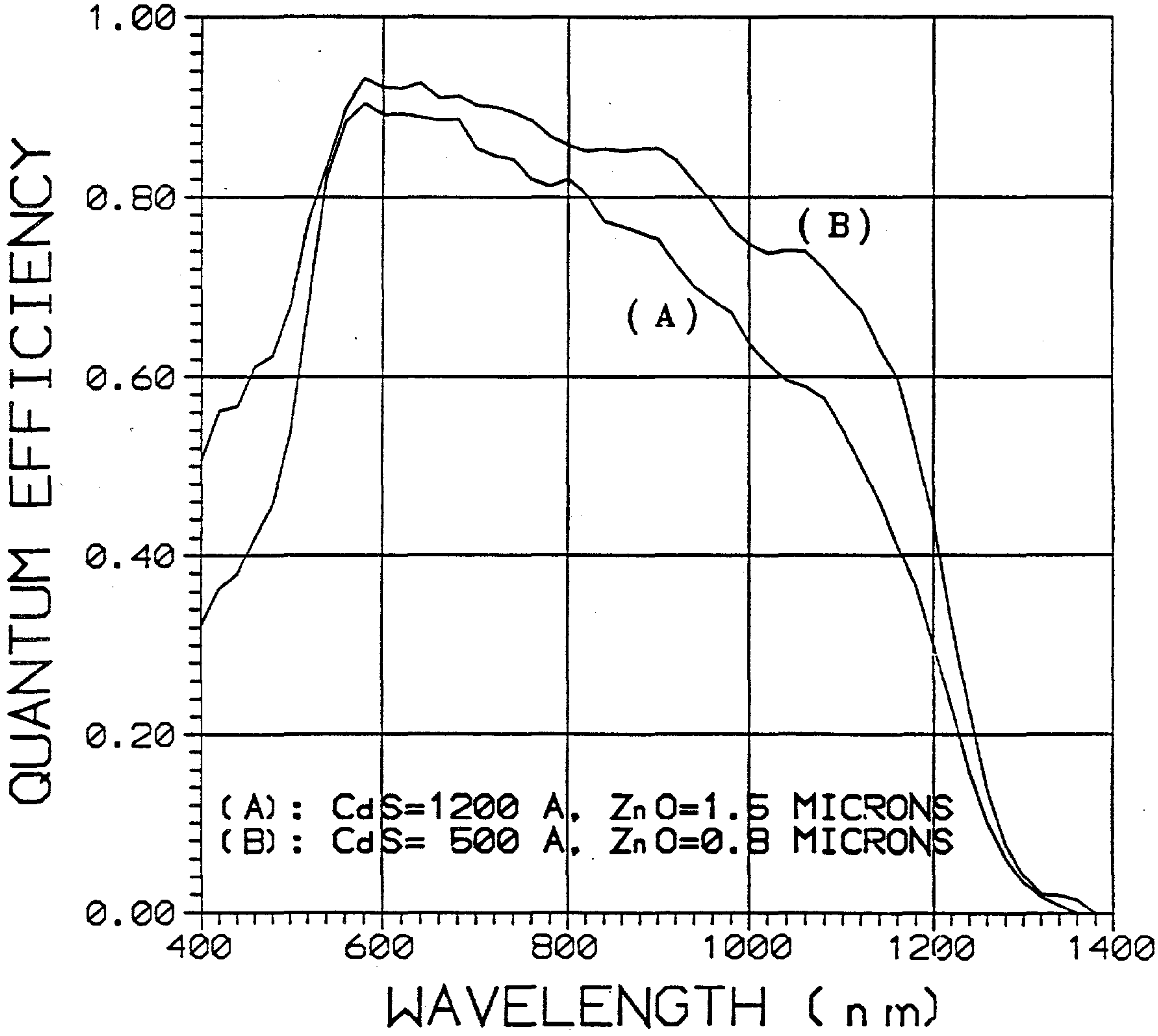

parasitic absorption losses both in the CdS layer as well as in the ZnO layer resulted in a net increase in current by about 5 mA/cm^2.

2.1.4.2 *Contacts, Substrates*

The molybdenum (Mo) back contact has been deposited on glass both by sputtering from a target and by e-beam evaporation. In both cases, 1 - 2 µm thick films exhibit good adhesion and the sheet resistance is about 30 µΩ/□ - 50 µΩ/□. Sputtered Mo films typically have small grains, on the order of 200 nm.

The front contact to CIS solar cells consists of a bi-layer of aluminum and nickel, both evaporated by e-beam through metal masks.

Glass substrates have been used for all the work reported here. Both Corning 7059 glass and soda-lime glass has been used. In the initial stages of this program we used Corning 7059 glass but have subsequently switched entirely to soda-lime glass.

3.0 TASK II: ABSORBER MATERIAL

3.1 Deposition System: Design and Description

The deposition system used in this research program was designed with two objectives in mind. First, the system should be capable of producing CIS films on several substrates in each deposition run. Second, it must be able to demonstrate proof-of-concept for a large area deposition system. The system was designed to form the CIS compound with a high degree of spatial uniformity as the elements were deposited. Due considerations of process speed, ease of control and simplicity were taken into account. Particular attention was paid to uniformity of both the deposition flux and the substrate temperature. The physical vapor deposition technique of three source evaporation has demonstrated that it is possible to achieve CIS compound formation during deposition. We use sputtering from elemental targets because it is easier to control the deposition process, it is easier to achieve uniformity over large areas, and more amenable to process scale-up.

During this period CIS film deposition has been explored by two physical vapor deposition methods. In the first method, copper, indium and selenium were sputtered from elemental targets onto substrates held at elevated temperatures. In the second method, the sputtering of selenium is replaced by thermal evaporation of selenium.

The deposition system used for this purpose has a single vacuum chamber and is pumped by an oil diffusion pump. The system has a liquid nitrogen (LN2) cold trap over the diffusion pump. The base pressure for the vacuum system is 10^{-7} Torr. The pressure is measured by a barometric and ion gauge. The sputtering gas flow is controlled by a needle valve. The heaters are controlled via thermocouples and standard proportional temperature controllers.

The system contains three magnetron sputtering sources. The magnetrons are arranged as shown in **Figure 3-1**. The magnetrons all sputter in a direction perpendicular to the plane in which they are mounted. Argon is used as the sputtering gas. Elemental sputtering targets are used in each magnetron. Commercially-available high-purity Cu and In sputtering targets are used. The Se sputtering target was designed and fabricated at Solarex by a proprietary process. The magnetrons are driven by independent power supplies. Independent power supplies allow independent control of the flux of each element. The deposition rate of each element is, by design, an independent experimental variable. The copper and indium magnetrons are driven by direct current power supplies, while the selenium magnetron is driven by a rf power supply. In order to achieve uniform films containing all three elements the substrates, which are mounted on a rotating substrate holder, move past each of the magnetrons. This holder is a disk which holds six, 3" x 3" substrates. The substrates pass over each sputtering target on each revolution of the

Figure 3-1. Schematic diagram of CIS deposition system.

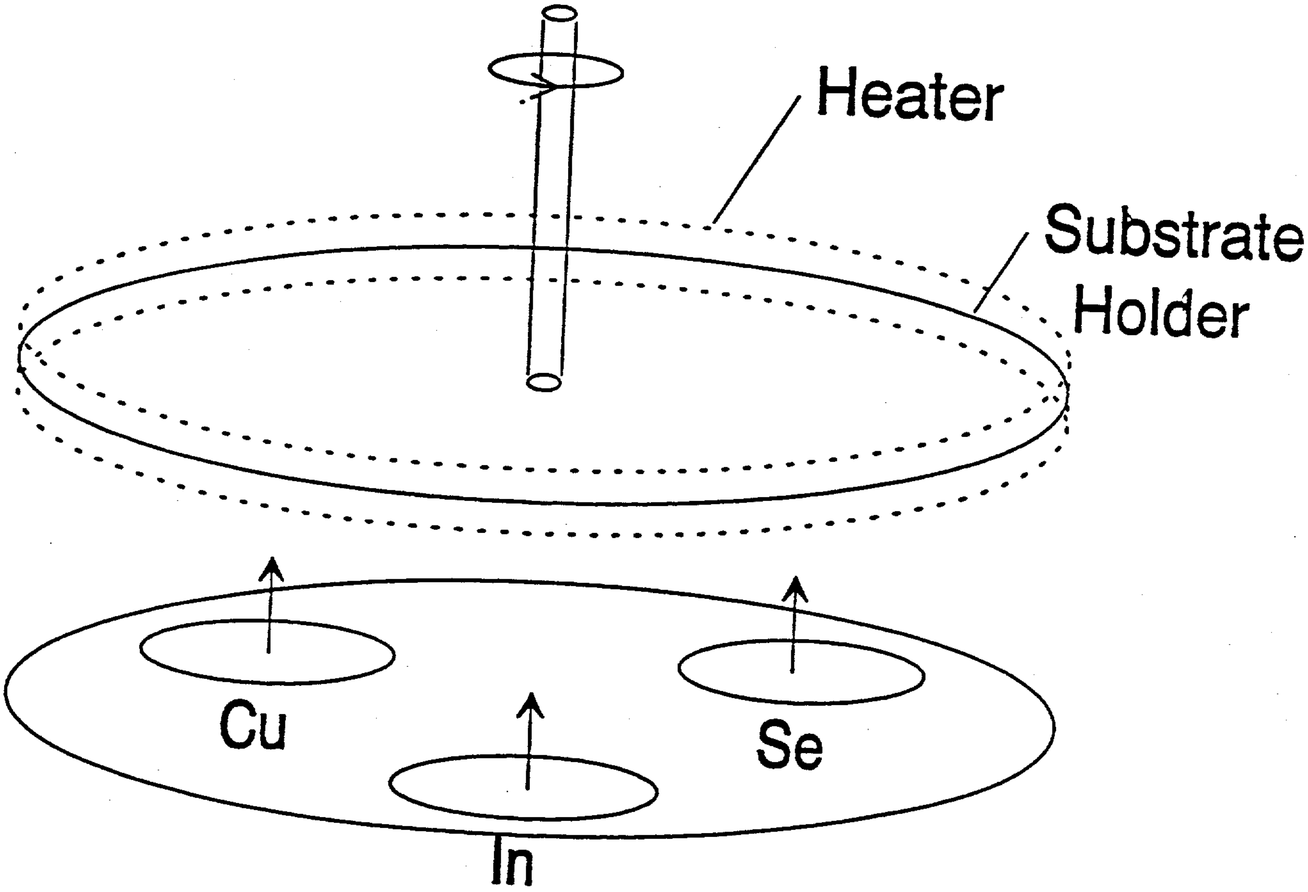

substrate holder. The deposition of the elements is simultaneous in the sense that the magnetrons are all operated at the same time. However, from the frame of reference of a particular substrate, the deposition is sequential. The amount of each element that reaches the substrate as the substrate passes over a magnetron during one rotation depends on the deposition rate and the angular velocity of the substrate holder. The substrate holder typically rotates at four to six revolutions per minute. During a one hour deposition, a film will be made up of 240 sets of In, Cu and Se layers. A typical film that is about two microns thick is made of sets of In-Cu-Se layers that have individual thickness of about 4 nm. The space between the magnetrons is about the same as the diameter of the magnetron. A substrate spends one-sixth of each revolution over each magnetron and one-sixth of each revolution in the space between each pair of magnetrons. The substrate receives each elemental flux one-sixth of the time and sees no deposition flux one-half of the time. The instantaneous deposition rate is six times larger than the time average deposition rate. In the discussion of deposition and film growth (*see* Section 3.3) the time average value has been used. The substrate is heated by thermal radiation inside an isothermal oven. Inside the vacuum system, a pillbox shaped oven just fits around the substrate holder. The substrate holder is supported by a shaft that also provides the rotation. The shaft enters the oven through a small hole on the top side. The deposition flux enters the oven through three holes on the bottom side of the oven. The substrate holder is completely surrounded by the oven except for these openings. The oven contains heaters which are both above and below the substrate holder. The wall of the oven consists of three separate walls which serve as radiant heat shields.

3.2 Calibration of Substrate Temperature

Direct measurement of the substrate temperature is not practical because the substrates are on a moving substrate holder. The temperature of the substrates is inferred from the temperature within the isothermal oven. In order to evaluate the correlation between the temperature of the oven and the temperature of the substrates, the temperature of a single substrate was measured while the substrate holder was stationary and the substrate was positioned adjacent to an opening. In this configuration the substrate was heated only from the top side. Measuring the substrate temperature while the substrate is stationary should give the worst case correlation. This is because when the substrate is rotating it is constantly heated from the top side and heated during one-half of the time from the bottom-side. For stationary measurements, the substrate receives only two-thirds of the normal thermal flux. The result of these measurements are summarized in **Table 3-1**.

Table 3-1. Substrate Temperature Calibration and Uniformity.

		Substrate	
Set Point	**Oven**	**Inside Edge**	**Outside Edge**
300	300	306	306
350	345	342	344
400	398	382	388
450	449	424	431
500	500	471	478

(Temperatures in °C)

These measurements show that both the variation across the substrate is small, and the correlation between actual and set point temperature is quite good. At 400°C, the difference between the set point and the average substrate temperature, is only 14°C. The variation across the substrate is only 6°C at 400 °C.

3.3 Calibration of Single Layers Cu, In, and Se

The deposition rates for the three individual elements (Cu, In and Se) were established by depositing one element at a time. This also allowed us to establish the extent of deposition parameters that can be used reproducibly. Six 3" x 3" substrates were mounted on the substrate holder for each deposition. The substrate material was soda-lime glass or Corning 7059 borosilicate glass. The soda-lime glass was used in the majority of the depositions. Glass substrates were coated with about 1.5 μm thick sputtered molybdenum. Mo films had small grains with characteristic dimensions of about 200 nm, typical for sputtered Mo. The sputtering gas used in all of these depositions was argon. Ar, atomic weight of 40, is lighter than both Cu (atomic weight 63.5) and In (atomic weight 115), so it is not the best choice to maximize the momentum transfer. However, it works satisfactorily. The choice of Ar pressure is a compromise between gas phase scattering of the sputtered flux and the operation of the magnetrons. Higher pressures result in more gas scattering. The mean free path is shorter and the transport of the sputtered flux to the substrates is poorer at higher pressures. The mean free path in cm is approximately 5/p where p is the pressure in mTorr. The distance from the magnetron to the substrate is on the order of 10 cm. This implies that a sputtering pressure of 1 mTorr of the magnetron is a distance of 2 mean free paths from the substrate. At a sputtering pressure of 5 mTorr the magnetron is a distance of 10 mean free paths from the substrate. As these numbers illustrate, minimizing the sputtering gas pressure makes significant difference in the transport of the sputtered flux to the substrate. On the other hand, the magnetrons have a minimum gas pressure for operation. As the gas pressure decreases the voltage required to operate the magnetron increases. For s-gun magnetrons that are used on this system, the voltage is unreasonably high at about 1.5 mTorr. Hence, the argon gas pressure used in these depositions was held between 1.5 and 2.0 mTorr.

One of the design considerations for this deposition system was to have a system that is easy to control. Magnetron sputtering of metals is easy to control because the sputtered flux is proportional to the current that is driving the magnetron. There are, however, deviations from this proportionality. If the magnetron target changes in some fundamental way, such as the target element changing oxidation state, then the ratio of current to flux will change but for a given set of conditions the deposition rate is proportional to the current. The deposition rate is tracked in terms of specific deposition rate, which is the time average film thickness deposited per unit time and unit current. The specific deposition rates listed in **Table 3-2** are rates determined by measuring the thickness of single element films.

Table 3-2. Specific Deposition Rate.

	In	Cu	Se	Se
Initial Values	0.31 (nm/amp-sec)	0.31 (nm/amp-sec)	0.63 (nm/amp-sec) for dc sputtering	3/5 (nm/kw-sec) for rf sputtering
Final Values	0.38 (nm/amp-sec)	0.12 (nm/amp-sec)	1.7 (nm/sec) for thermal evaporation	

The differences between the initial and final values of the In and Cu specific deposition rate is due to the installation of a new target or substantial target erosion. The three values for Se specific deposition rate represent three methods of depositing Se. The surface morphology of single layer films show that Cu and Se form smooth homogenous films. Indium films, however, usually form textured films. The surface morphology has a characteristic dimension of about 1 micron. When Cu and In are deposited simultaneously, the resultant films is textured.

3.4 Deposition and Characterization of CIS Films

Table 3-3 summarizes the typical deposition conditions. These are conditions that have resulted in good compositions in CIS films. The films are typically deposited by simultaneously sputtering all three elements onto heated substrates. The Cu and In currents are varied so that the initial portion of the films has a Cu-rich flux and the final portion of the film has a Cu-deficient flux.

Table 3-3. Typical Deposition Conditions.

6 substrates	sputtered Mo on 7059 and soda-lime
sputtering gas pressure	1.5 to 2.0 mTorr
substrate temperature	350°C to 475°C
Cu sputtering current	0.200A to 0.350A
In sputtering current	(.600A to .750A first target) .300A new target
Se sputtering current	60W to 70W for rf sputtering
Se thermal evaporation	source operated at 375°C

CIS Films #105, #106, #108, and #110 illustrate several important aspects of CIS deposition by three source sputtering. The composition of these films is tabulated in **Table 3-4**.

Table 3-4. Composition of Several Sputtered CIS Films.

Sample #	% Cu	% In	% Se
105-1-2	22.3	25.8	51.9
106-4-2	22.7	24.8	52.6
108-4-5	23.5	24.2	52.3
110-5-5	24.6	22.9	52.5

Figure 3-2 (a),(b),(c),(d) shows the common difference between the Cu-deficient and Cu-rich films. The Cu-rich film (#110) has large grains with well-defined facets. The other three films are Cu-deficient and have small grains and no well-defined facets.

The Cu-deficient films (#105 and #106) also show interesting anomalous growth. Film #105 has very long continuous features often referred to as "worms". Film #106 has more symmetrical features often referred to as "boulders". These features are distinctly different from the rest of the films which are characterized by a regular bumpy surface composed of small grains. The anomalous features occur very regularly across the films, which suggests that these features are an intrinsic feature of the film rather than caused by some external factor such as film contamination. EDX analysis of the anomalous features show near stoichiometric composition.

Figure 3-2. SEM photomicrographs of samples a) 105, b) 106, c) 108, d) 110 showing variations in grain size and morphology of CIS films.

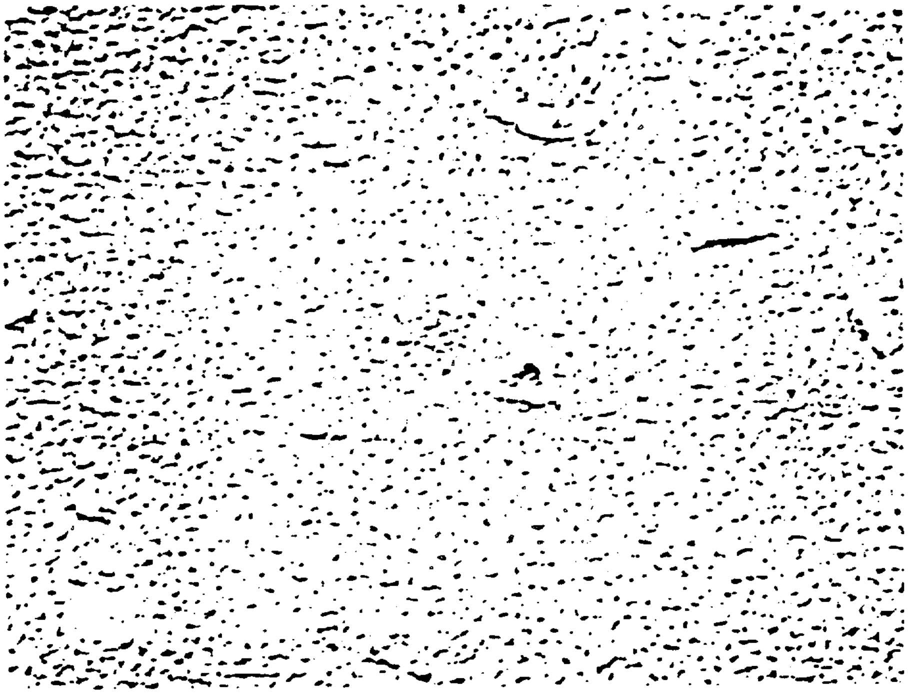

(a)

Figure 3-2 (continued).

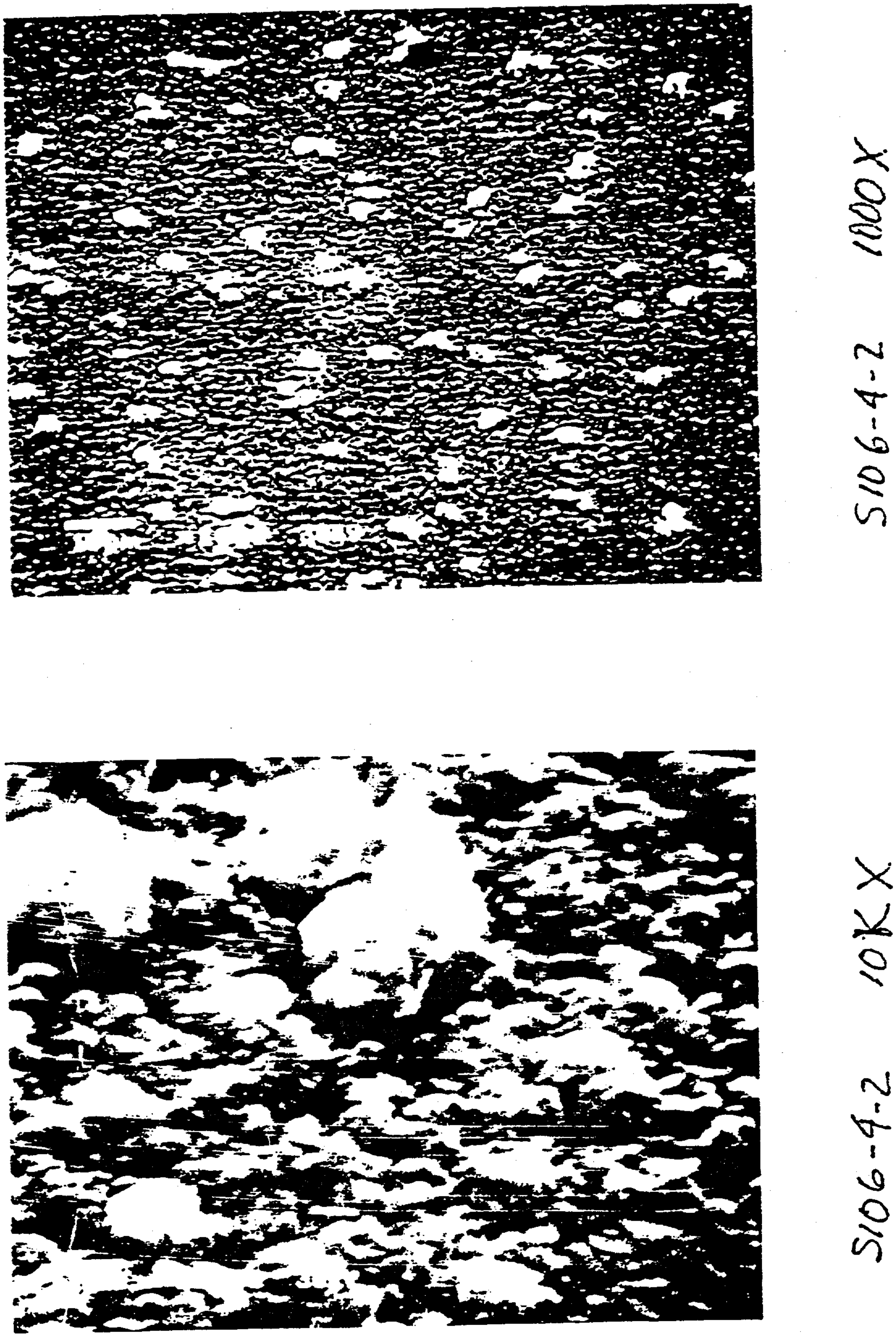

(b)

Figure 3-2 (continued).

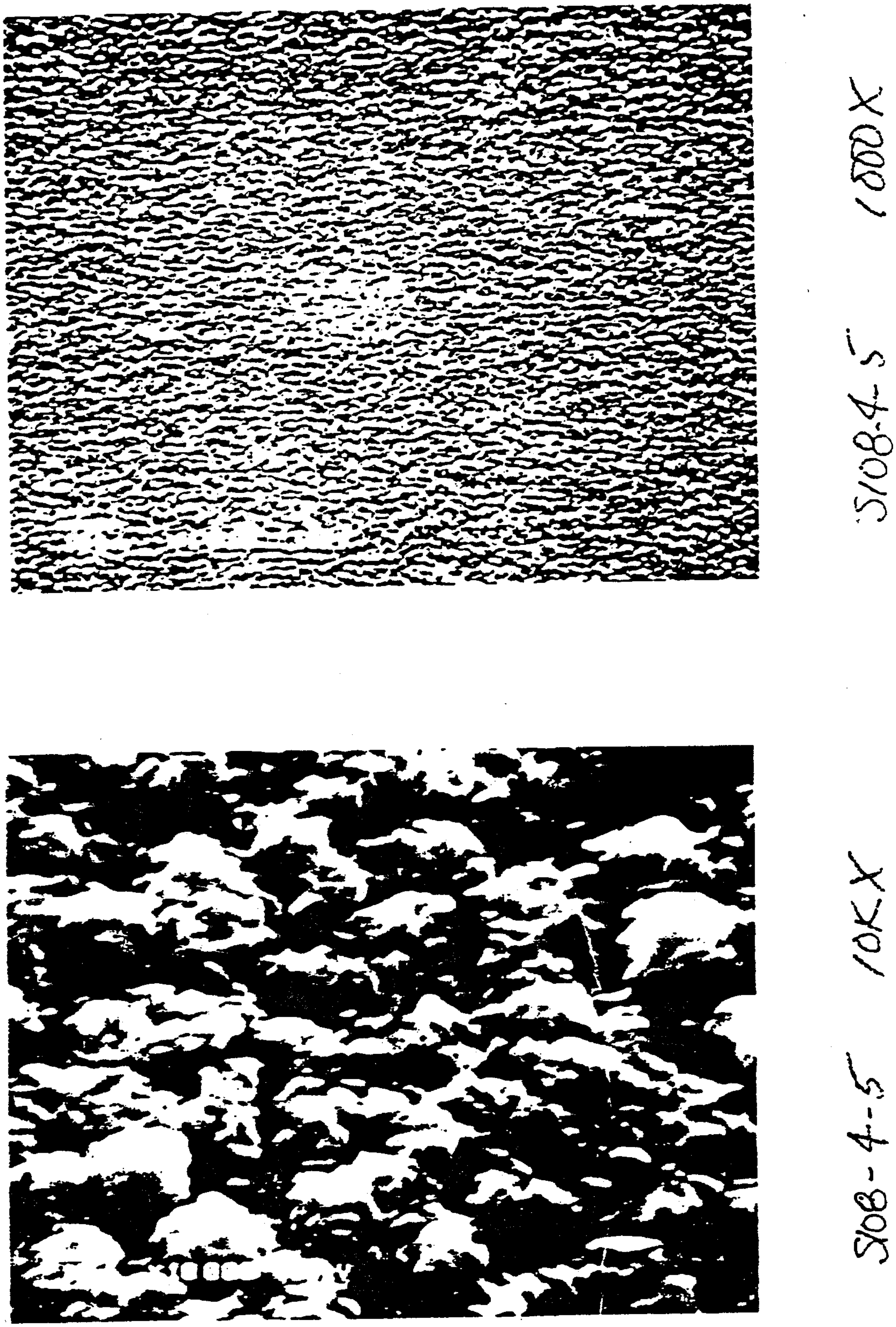

(c)

Figure 3-2 (continued).

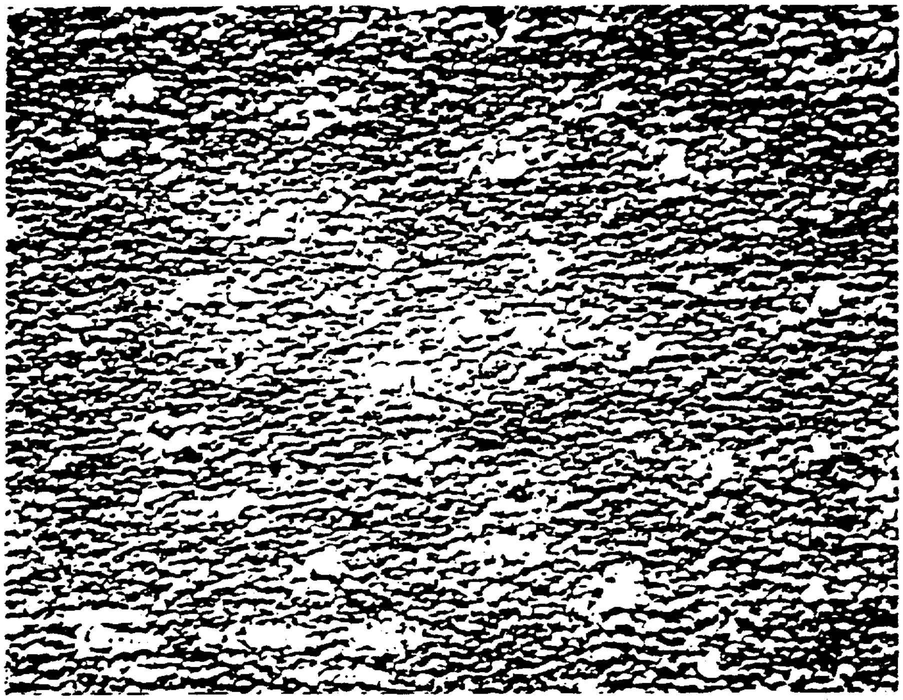

S110-5-5 1000X

(d)

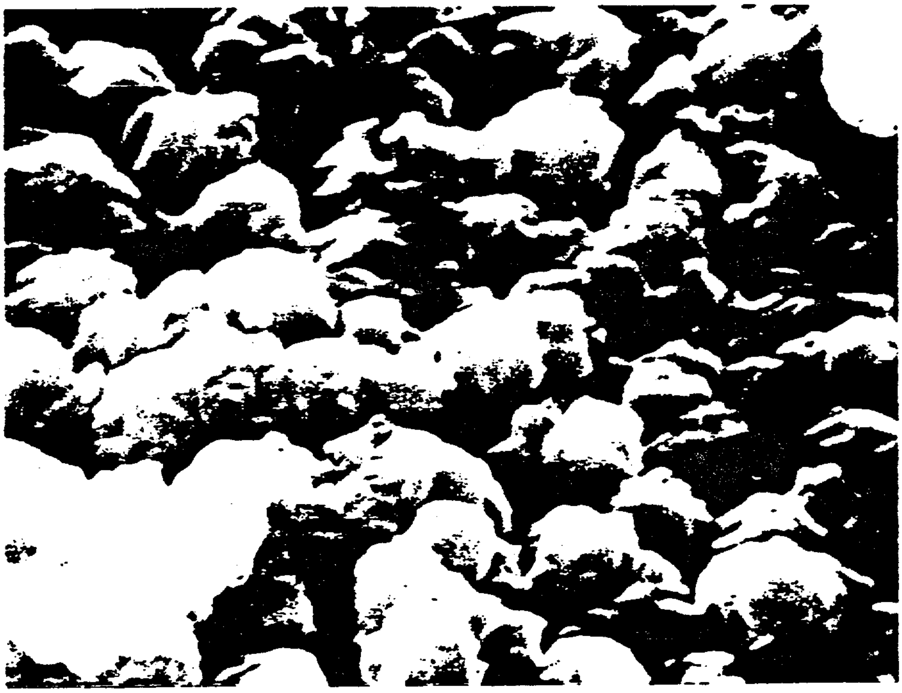

S1105-5 10KX

All of the above films are two-layer films, except for #110, which is a single layer film. The first layer is deposited as Cu rich at 300°C to 350°C and at a low sputtering rate. The second layer is deposited as Cu-deficient at 450°C to 500°C and at a moderate sputtering rate. Film #110 which is Cu rich was deposited with the conditions for Cu-deficient second layers. Film #110 is another example of devious behavior by the deposition system. The reproducibility of the previous depositions suggests that the specific deposition rate was not changing and that the unexpected composition may be caused by loss of In from the growing film as happens during the deposition of In-rich CIS films by reactive sputtering. The idea that there is loss of In during deposition is supported by the fact that the specific deposition rate multiplied by the typical deposition current gives a very different deposition rate for Cu and In. The calculated deposition rate is much higher for In than for Cu. Reduction of the flux due to Se contamination is also a possibility but Se contamination should reduce the Cu flux more than the In flux.

3.5 Effect of Substrate Temperature

We have studied the effect of substrate temperature on the composition and morphology of single layer CIS films and sequentially deposited CIS films.

Three single layer films were deposited with the same deposition conditions. The average compositions and substrate temperatures are listed in **Table 3-5**. The only clear trend in the composition data is that the Se content increases as the substrate temperature increases. The composition data is normalized so trends in the ratio of compositions is instructive. The Cu/In ratio decreases with increasing temperature. The (Cu + In)/Se ratio decreases with increasing temperature, which is concomitant with the Se increase. Despite the high vapor pressure of the Se, higher temperatures promote higher Se concentrations.

Table 3-5. Temperature Effect on Single Layer Films.

Sample #	Temp.	% In (s)	% Cu (s)	% Se (s)	Cu/In	(Cu+In) /Se
116	470°	23.4 (0.19)	22.2 (0.17)	54.4 (0.18)	0.95	0.84
118	450°	23.2 (0.54)	23.0 (0.52)	53.7 (0.41)	0.99	0.86
119	410°	23.4 (0.51)	23.8 (0.18)	52.9 (0.42)	1.02	0.89

Note: The averages are calculated over six separate EDX analyses with collection times of 100 (live) seconds each. Compositions are atomic % and are normalized before averaging. (s) is the sample standard deviation.

The variation in the Cu/In ratio appears clear. However, the differences between the In values and the Cu values are not all statistically significant. The apparent trend in the Cu/In ratio is not conclusively indicative of any particular trend and does not match subsequent observations.

We have also studied the effect of substrate temperature on the composition of films made by sequential deposition of Cu, In and Se. CIS films were made by sequentially depositing the three elements onto heated substrates at various temperatures. **Table 3-6** lists the composition of four films that were deposited under identical conditions except for the temperature of the substrate. The most striking feature of this data is that at low temperature, 330°C, the In content is extremely high and the Se content is extremely low. The low Se content is due to two factors. The flux of Se is sensitive to the ambient temperature, decreasing at low temperature, and the reactivity of Se decreases at low temperature. The cause of the In variation is not apparent from the data. In loss at high temperature is one possible explanation. The Cu/In ratio appears to follow a trend that is opposite the trend seen in **Table 3-5**. With the exception of the 330°C data the variation may not be significant. The trend in the (Cu+In)/Se ratio is the same as the trend seen previously and is concomitant with the Se variation. The repetition of depositions at 400°C show the reproducibility of the deposition and analysis. The major trends are easily observed. However, the reproducibility or accuracy of either the deposition or the analysis is not sufficient to definitively evaluate the subtle change in the Cu and In content at the higher temperatures.

Table 3-6. Effect of Substrate Temperature on Films of Sequentially Deposited Elements.

Sample #	Temp.	% Cu (s)	% In (s)	% Se (s)	Cu/In	(Cu+In) /Se
122	470°	22.2 (1.40)	23.8 (0.90)	53.9 (0.70)	0.93	0.86
125	400°	22.7 (0.74)	26.0 (0.34)	51.3 (0.56)	0.87	0.95
124	400°	22.2 (0.23)	26.6 (0.47)	51.1 (0.58)	0.84	0.95
123	330°	24.6 (2.08)	40.0 (2.48)	35.4 (1.75)	0.62	1.83

3.6 Temperature Effect on Cu-In Films

To determine cause of the radical variation in In content in CIS films deposited at different substrate temperatures, three films of just Cu and In were deposited. The results show the same large excess of In at low temperature. However, the temperature at which the large excess shows up is at 30°C rather than 330°C. All of these films have very irregular morphologies. Upon close inspection, it is clear that the In is segregated at the surface of the film when deposited at low temperature. Spot analysis by EDX gives very different results for Film # 127 than the usual area average. The background material measures 45% Cu and 55% In while the large grains that appear to sit on the surface of the film measure 14% Cu and 86% In. These measurements are not precise because the film is very rough and the excitation volume is larger than the target volume, but the difference in the measurement is so distinct that it is clear that the In has segregated to the surface. At the higher substrate temperatures, the films measure essentially 50% Cu and 50% In.

A sample of #127 was heat treated at 400°C. This temperature is below the melting temperature of the CuIn alloy. The morphology of the film did not change, indicating that there was no overt alteration of the film. Composition measurement of the film, after heat treating, gives values that are significantly closer to the expected result of 50% Cu / 50% In. Diffusion during the heat treatment moderated the segregation.

Table 3-7. Effect of Substrate Temperature on Cu-In Films.

Sample	Temperature	% Cu (s)	% In (s)	Cu/In
127	30°	36.2 (0.84)	63.7 (1.06)	0.6
128	250°	49.9 (1.37)	49.9 (1.37)	1.0
129	400°	52.3 (3.86)	47.4 (3.89)	1.1
127 large grain	30°	14.4	85.6	0.2
127 background	30°	44.7	55.1	0.8
127 after heating	400°	40.9	58.5	0.7

The extremely high values measured for In in some films results from segregation of In to the surface. Segregation may also significantly perturb other measurements. Indium can segregate or it can be lost. Its incorporation into films is complicated.

3.7 Correlation of Composition and Morphology

Samples from #135 and #137 shown in **Figure 3-3 (a), (b), (c), (d), (e)** show the variation of morphology for single layer films as a function of film composition. The In-rich films are relatively smooth and have small grains on a micron scale. The Cu-rich films are rough and have

Figure 3-3. SEM micrographs showing changes in morphology of CIS films as a function of composition.

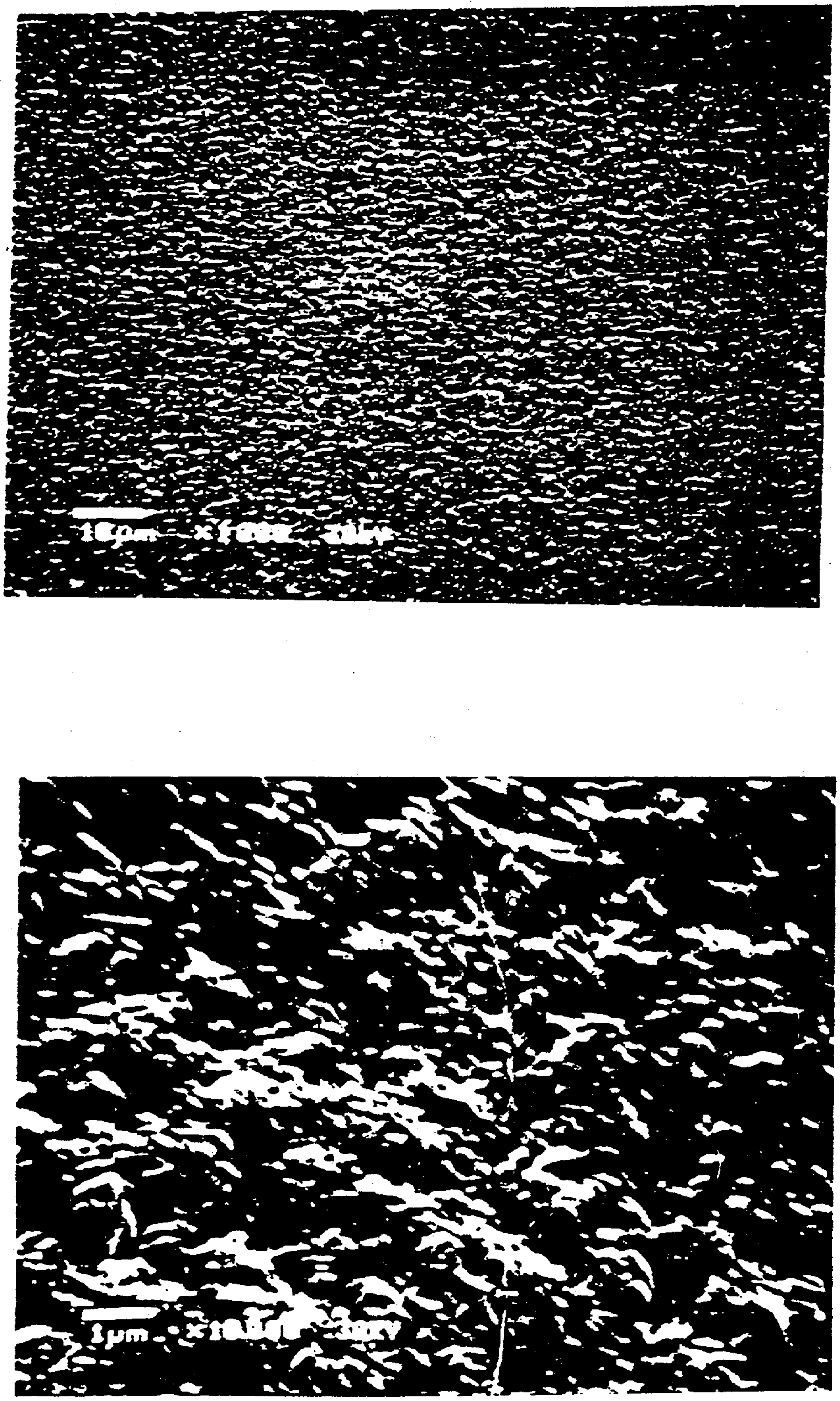

(a)

Figure 3-3. (continued)

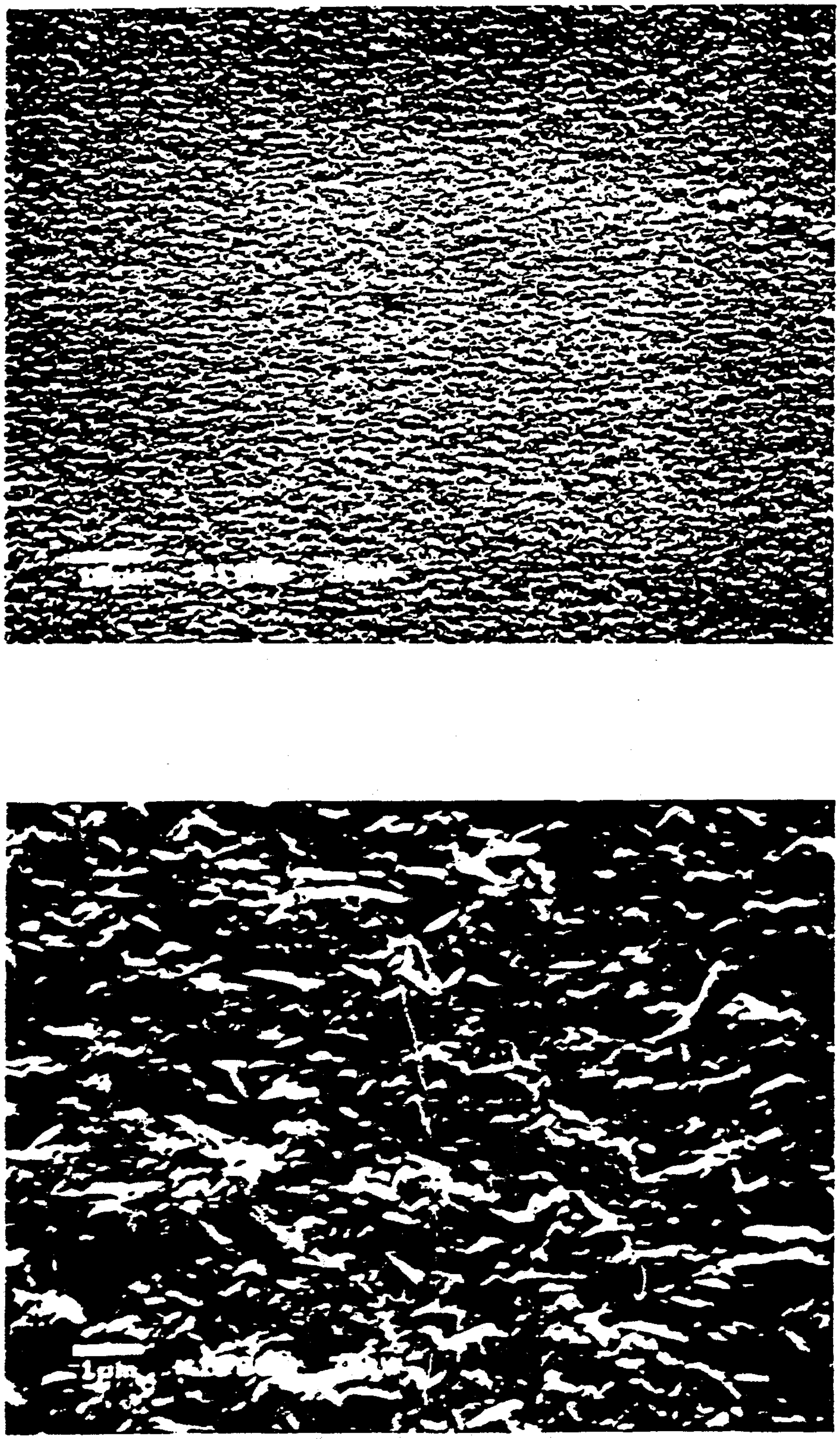

(b)

: b) 137-4-5 23.3% Cu, 23.9% In, 52.8% Se, Cu/In=0.98

Figure 3-3. (continued)

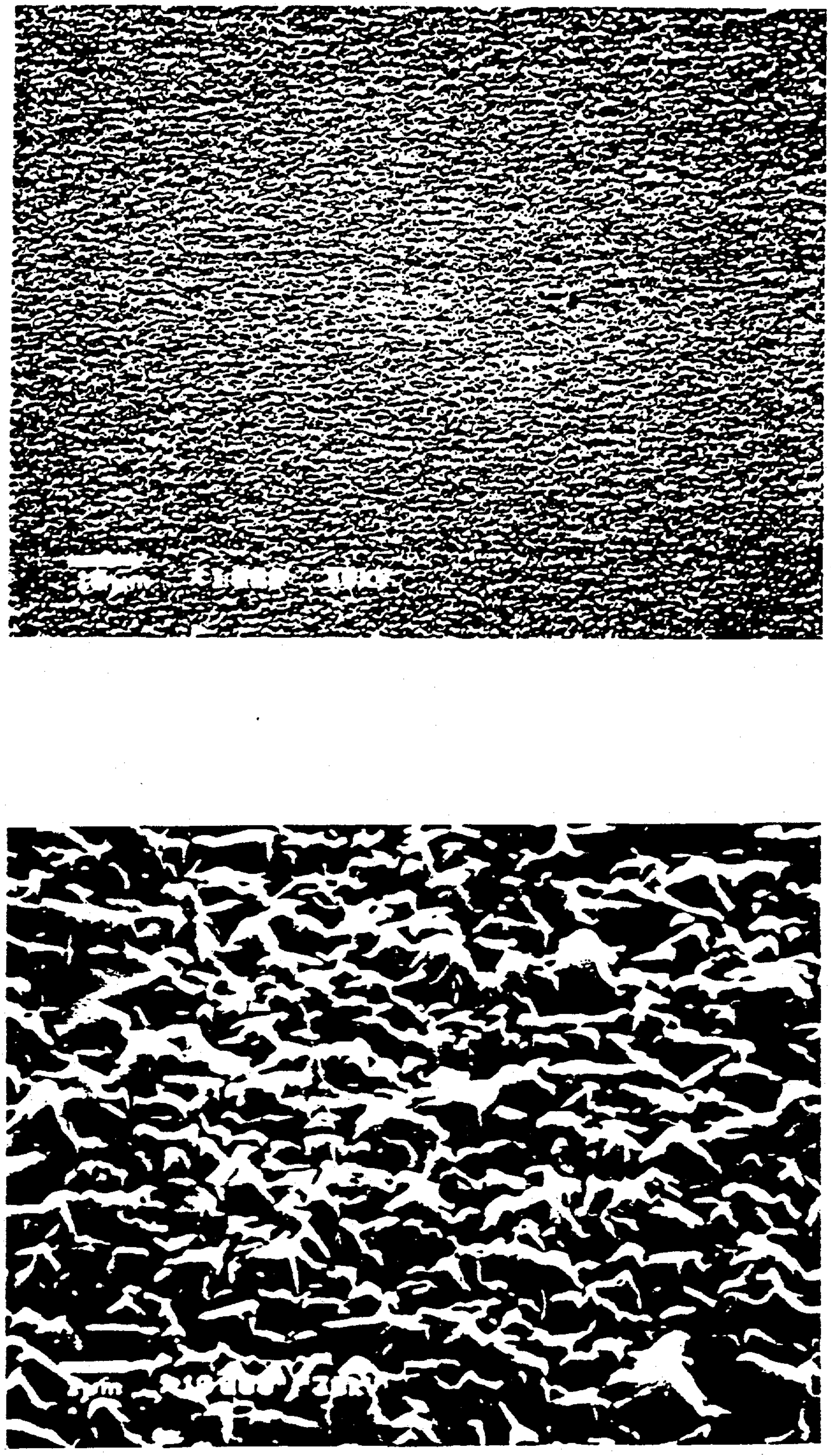

(c)

c) 135-4-8 24.4% Cu, 23.4% In, 52.3% Se, Cu/In=1.04

Figure 3-3. (continued)

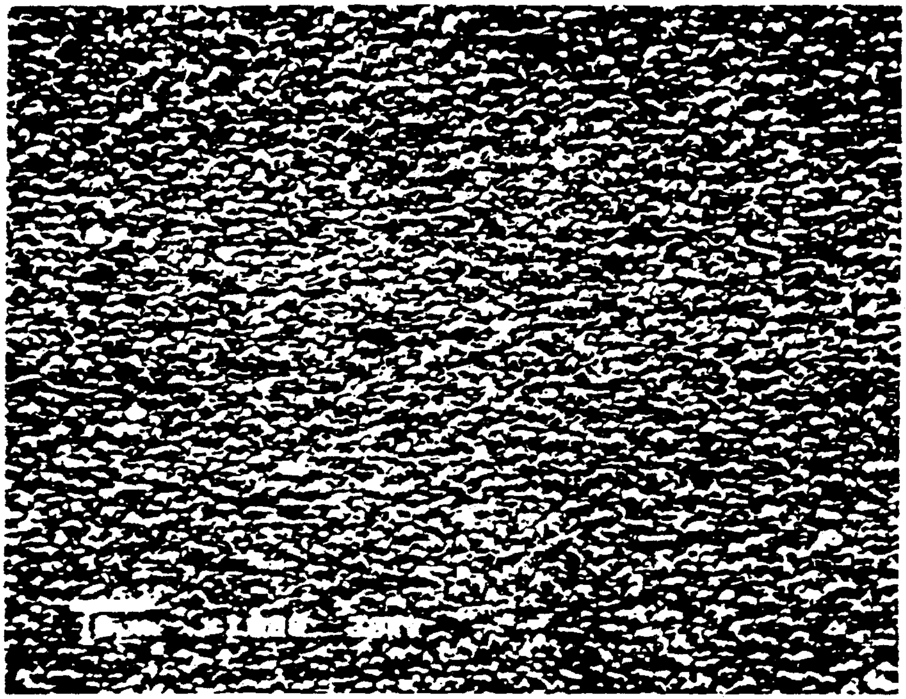

(d)

d) 135-4-5 25.7% Cu, 22.3% In, 52.0% Se, Cu/In=1.15

Figure 3-3. (continued)

(e)

e) 135-4-2 27.4% Cu, 20.9% In, 51.7% Se, Cu/In=1.31

large grains with well-defined facets. To be more exact, the morphology correlates to the Cu/In ratio. Film 135-4-8 has less than 25% Cu but the Cu/In ratio is greater than 1.0 and the grains are large and faceted.

3.8 Problems with Sputtering Se

One of the severe problems with the control of our deposition system has been variation in deposition rate. The specific deposition rate for each element was calculated from CIS film thickness and composition. The calculations yield widely varying results as seen in **Table 3-8**.

Table 3-8. Specific Deposition Rate Variation.

Run #	Cu	In	Se	Temperature
S132	2.1	1.9	36	---/475
S144	2.5	1.3	29	470/475
S145	1.6	1.8	28	477/475
S146	1.4	2.3	40	470/460
S153	2.1	2.2	52	473/475
S156	2.8	1.8	35	466/475
S157	1.9	1.4	29	469/475
S161	1.6	1.8	35	467/475
S162	1.2	1.5	35	443/450

The films from which the specific deposition rates were calculated have widely varying compositions as measured by EDX. The deposition parameters for all these films were chosen to give stoichiometric composition. The variation is due to changes in the deposition rate of the constituent elements. These changes are due to Se reacting with the Cu and In targets and diminishing the sputtering rate. The selenides that form on the targets subsequently sputter off and the sputtering rate increases.

The composition measurements are normalized so changes in any one of the three specific deposition rates causes a corresponding change in the other two values. Direct comparison of any one value with the subsequent value is not necessarily proportional to the change in the specific deposition rate. The Se specific deposition rate as calculated is not expected to be constant. The Se content is self-limiting. Se is intentionally deposited in excess to assure that sufficient Se is available for the growing film, and the excess evaporates. Se has a significant vapor pressure at the Se deposition temperatures. As a result, the Se in the film is not directly dependent on the true specific deposition flux. A large excess of Se adversely affect the material so the Se flux is limited to just slightly more than what is required to form stoichiometric CIS films. Excess Se in the system does adversely effect the control of Cu and In sputtering rates. Hence, the control of Se is critical. The original design of the system had assumed that a moderate excess of Se would supply sufficient Se for the CIS film and not be a problem. The design of the Se sputtering source mitigated the problems of controlling Se sputtering but did not eliminate the problems. Se has a low enough thermal conductivity (10^{-5} cal/s.cm.°C, Cu is 0.94) and a high enough vapor pressure (1 Torr at 350°C, Cu and In are less than 10^{-11} Torr at 350°C) that Se evaporates as well as sputters. The total Se flux is a function of temperature. Because the current density in a magnetron plasma increases with gas intensity, hot spots tend to develop on the Se target leading to excessive flux rates. These hot spots can also perturb the spatial uniformity of the films.

3.8.1 Thermal Evaporation of Se

A direct solution to the problems of Se sputtering, which is easier than Se target design, is to evaporate Se. The Se magnetron has been replaced by an Se thermal evaporator. The problems associated with the evaporator are precise temperature control, timing the heat up and shielding the system to avoid Se contamination of the Cu and In targets during heat up and cool down.

4.0 TASK III: DEVICE STRUCTURE

4.1 CIS Solar Cells

CIS solar cells have been fabricated with two device structures:

(i) Light => Ni-Al grid / ZnO / thin CdS / CIS / Mo / Glass
(ii) Light => Ni-Al grid / ITO / thick CdS / CIS / Mo / Glass

Most of the solar cells reported here have been fabricated with device structure (i) where all the layers are deposited at Solarex. The device structure (i) is shown in **Figure 4-1.** Device structure (ii) has been employed by IEC on CIS material deposited at Solarex.

In device structure (i), the procedure followed to fabricate devices is as follows: After the CIS layer has been deposited on Mo coated glass substrates, the CIS layer is coated with a thin CdS layer deposited by chemical solution growth and a thin ZnO layer deposited by LPCVD. A current collection metal grid is then deposited by e-beam evaporation. The solar cells are delineated by either lithography and etching or by mechanical scribing.

The photovoltaic parameters of devices fabricated on sputtered CIS are tabulated in **Table 4-1.**

Table 4-1. Photovoltaic Parameters of Some CIS Solar Cells.

Sample #	V_{oc} (mV)	J_{sc} (mA/cm^2)	FF	η (%)	Active Area
S132-2-2-252	344	32.2	56.8	6.3	0.074
S132-2-2-252	346	31.3	56.8	6.2	0.074
S132-2-2-251	343	31.9	56.2	6.2	0.074
S132-222-301	335	28.16	53.64	5.78	
S132-222-302	335	27.86	53.99	5.77	
S132-222-303	337	27.67	53.92	5.75	
S132-43-52	298	32.9	56.5	5.54	
S132-43-57	286	29.9	53.5	4.56	
S114-2-2-54	300	25.5	58.2	4.5	0.15
S309-5RS2	240	35.0	38.2	3.2	0.038

Figure 4-1. Schematic diagram of CIS solar cell device structure.

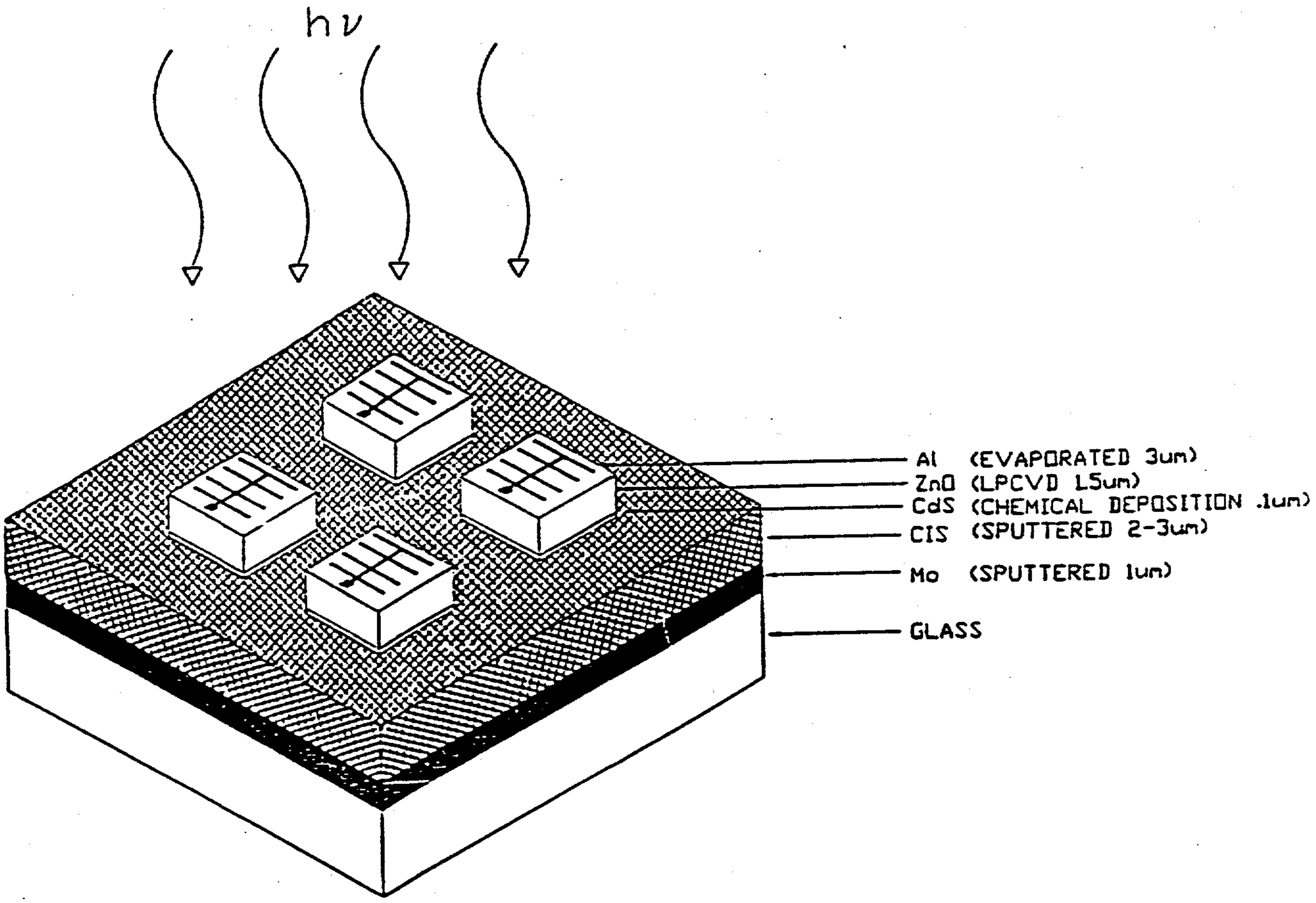

On sputtered CIS films, the best device fabricated with structure (i) had a conversion efficiency of 5.5% with the following parameters:

$$V_{oc} = 0.298V, J_{sc} = 32.9 \text{ mA/cm}^2 \text{ and FF} = 0.565$$

The window layer of this device comprised of CdS = 1100Å and ZnO = 1.5 μm with high dopant gas flow. The current is low in this device mainly due to absorption losses in CdS (short wavelength) and ZnO (long wavelength).

The best device (Sample # S132-2-2-251) fabricated at IEC employing device structure (ii) on sputtered CIS had a conversion efficiency of 6.2% with the following parameters:

$$V_{oc} = 0.343V, J_{sc} = 31.9 \text{ mA/cm}^2 \text{ and FF} = 0.562$$

Since this device had a thick CdS window layer there is no response at wavelengths below 500 nm. The gains in current at long wavelengths are negated by the short wavelength losses. **Figure 4-2** and **4-3** show the J-V characteristics and the corresponding quantum efficiency measurements of this device.

The best device (Sample # S189-5-1-S6) prepared on CIS prepared by sputtering/evaporation with device structure (i) also had a conversion efficiency of 6.2% but with the following parameters:

$$V_{oc} = 0.373V, J_{sc} = 35.5 \text{ mA/cm}^2 \text{ and FF} = 0.474$$

Figures 4-4 and **4-5** show the J-V characteristics and the corresponding quantum efficiency of this device. The relatively high current in this device is attributed to optimization of the window layer which is demonstrated by improvements in both the short wavelength and the long wavelength response of the device. The reasons for low fill factor are not clear. This method of preparing CIS by sputtering/evaporation is in its early stages of development. The initial results are encouraging because of the relative good values of V_{oc} and J_{sc}.

4.2 Quantum Efficiency Apparatus

A quantum efficiency apparatus has been designed and assembled. A schematic diagram of the apparatus is shown in **Figure 4-6**. The instrument used to measure the quantum efficiency of Solarex's CIS was built in-house from off-the-shelf components. The heart of the system is an H-20 monochrometer manufactured by Instruments SA, Inc. The spectral range is 400 nm to 1600 nm using a single grating. The single grating eliminates the possibility of an error when

Figure 4-2. J-V characteristics of 6.2% cell on sputtered CIS.

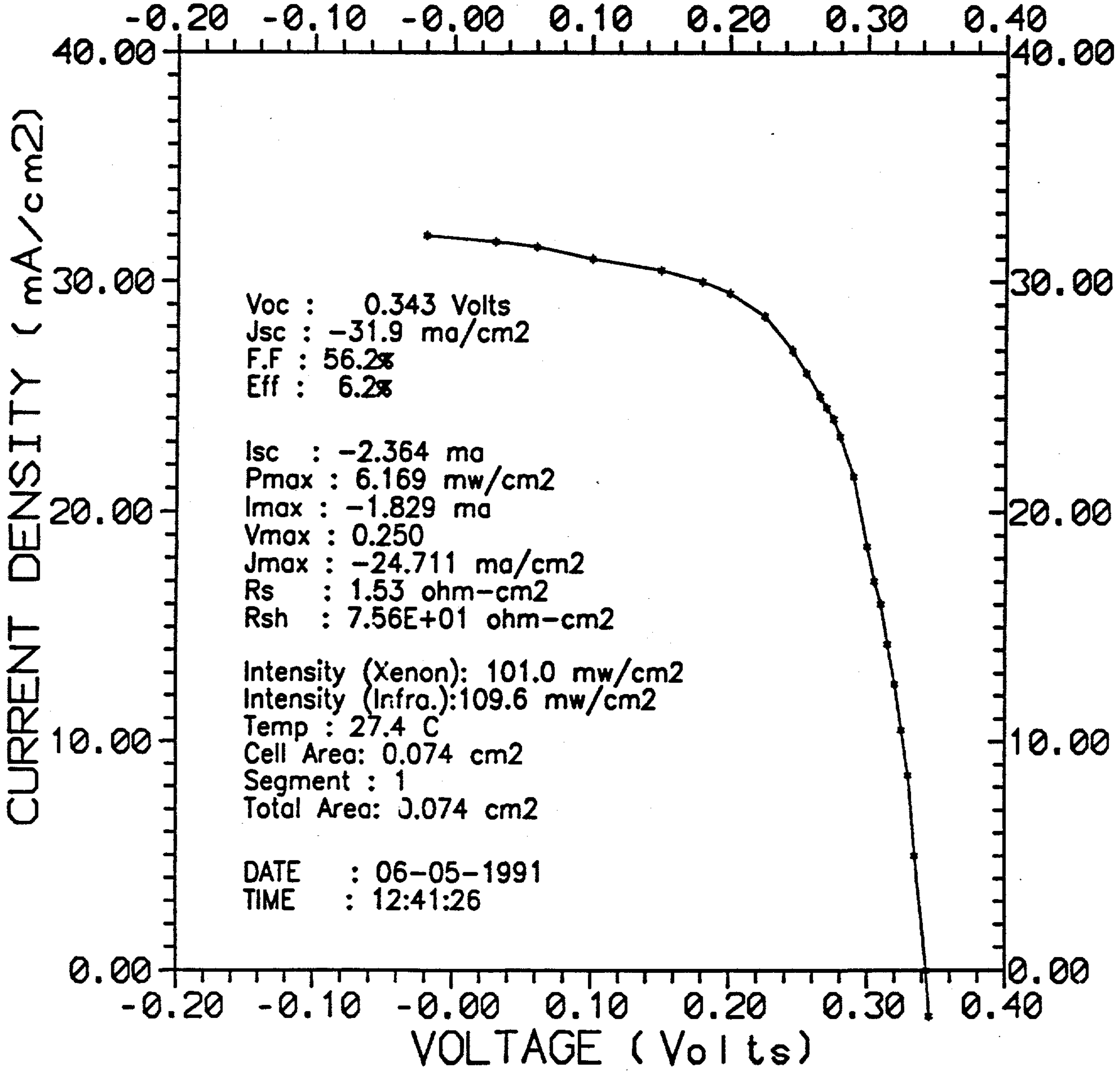

Figure 4-3. Quantum efficiency versus wavelength measurements of cell in **Figure 4-2.**

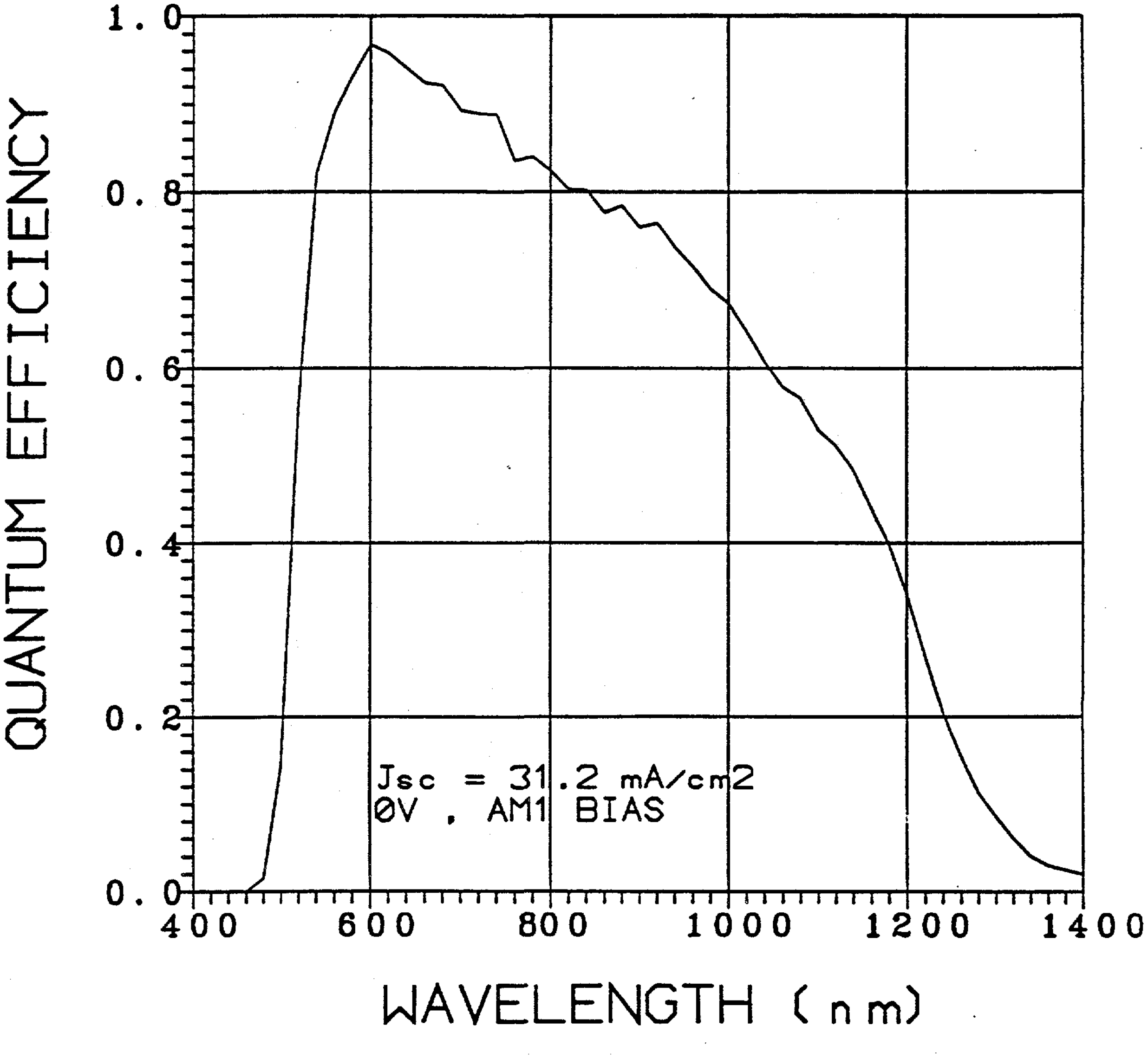

Figure 4-4. J-V characteristics of 6.2% cell on sputtered/evaporated CIS.

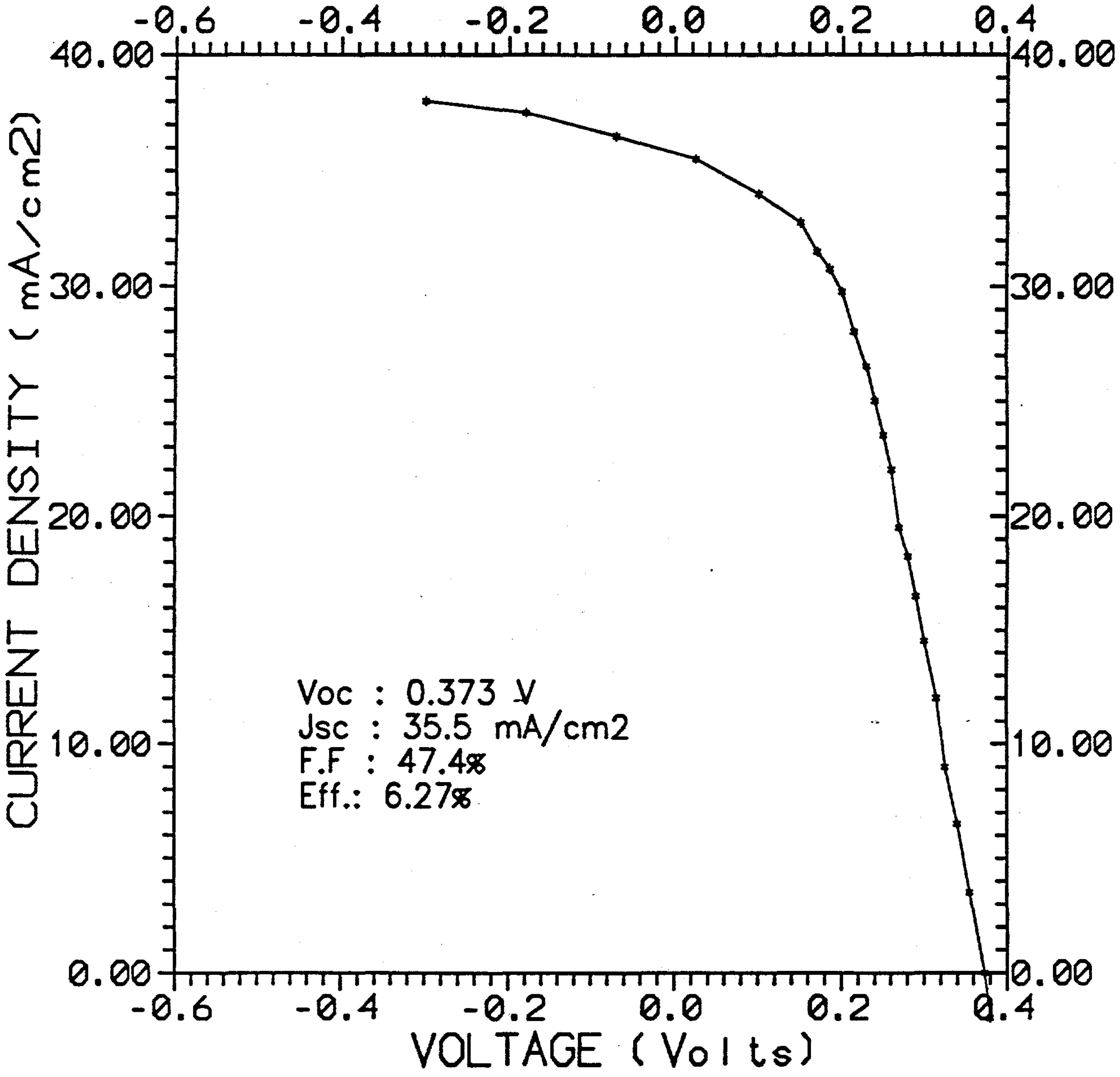

Figure 4-5. Quantum efficiency versus wavelength measurements of cell in **Figure 4-4.**

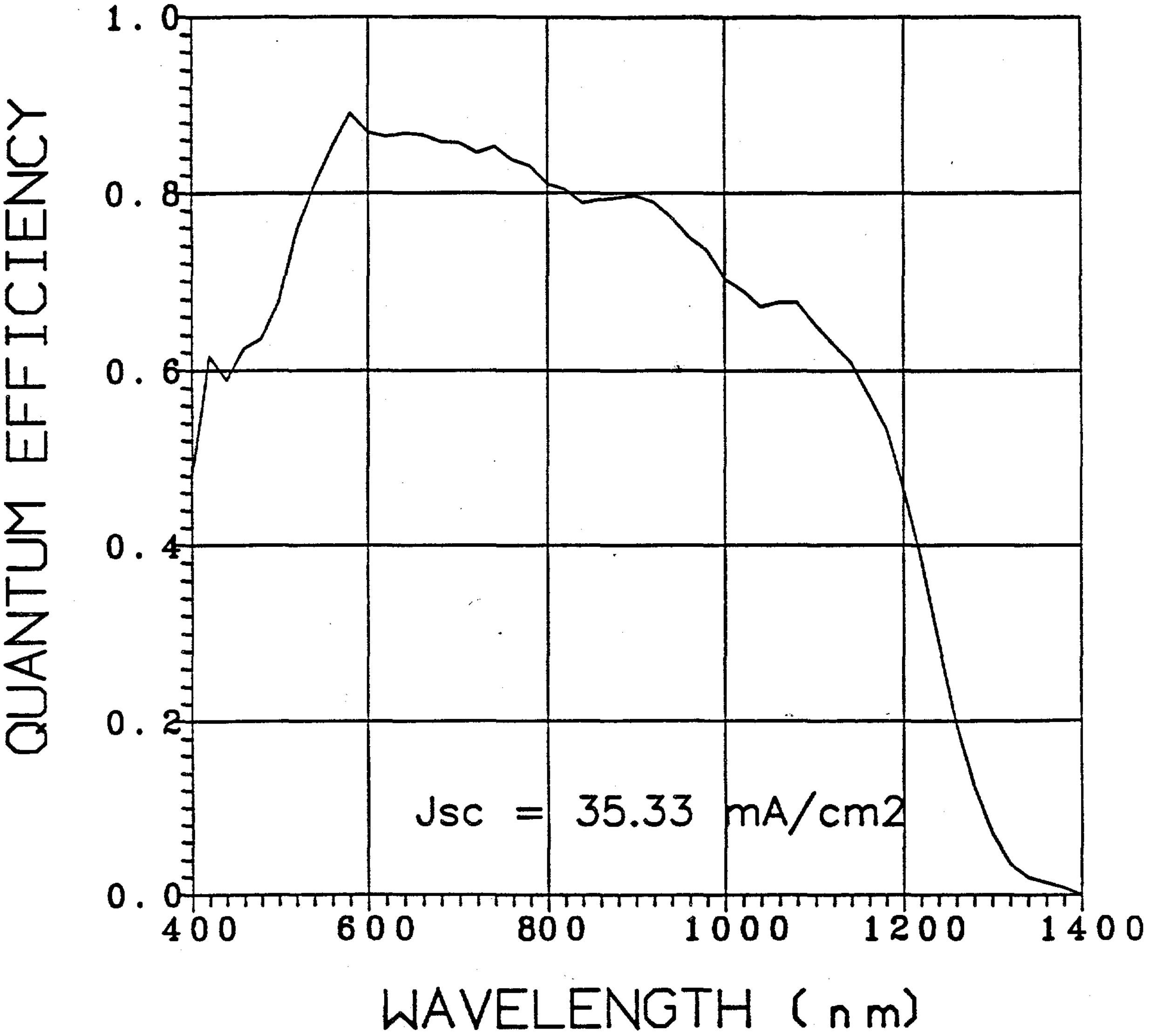

Figure 4-6. Schematic diagram of quantum efficiency measurement set-up.

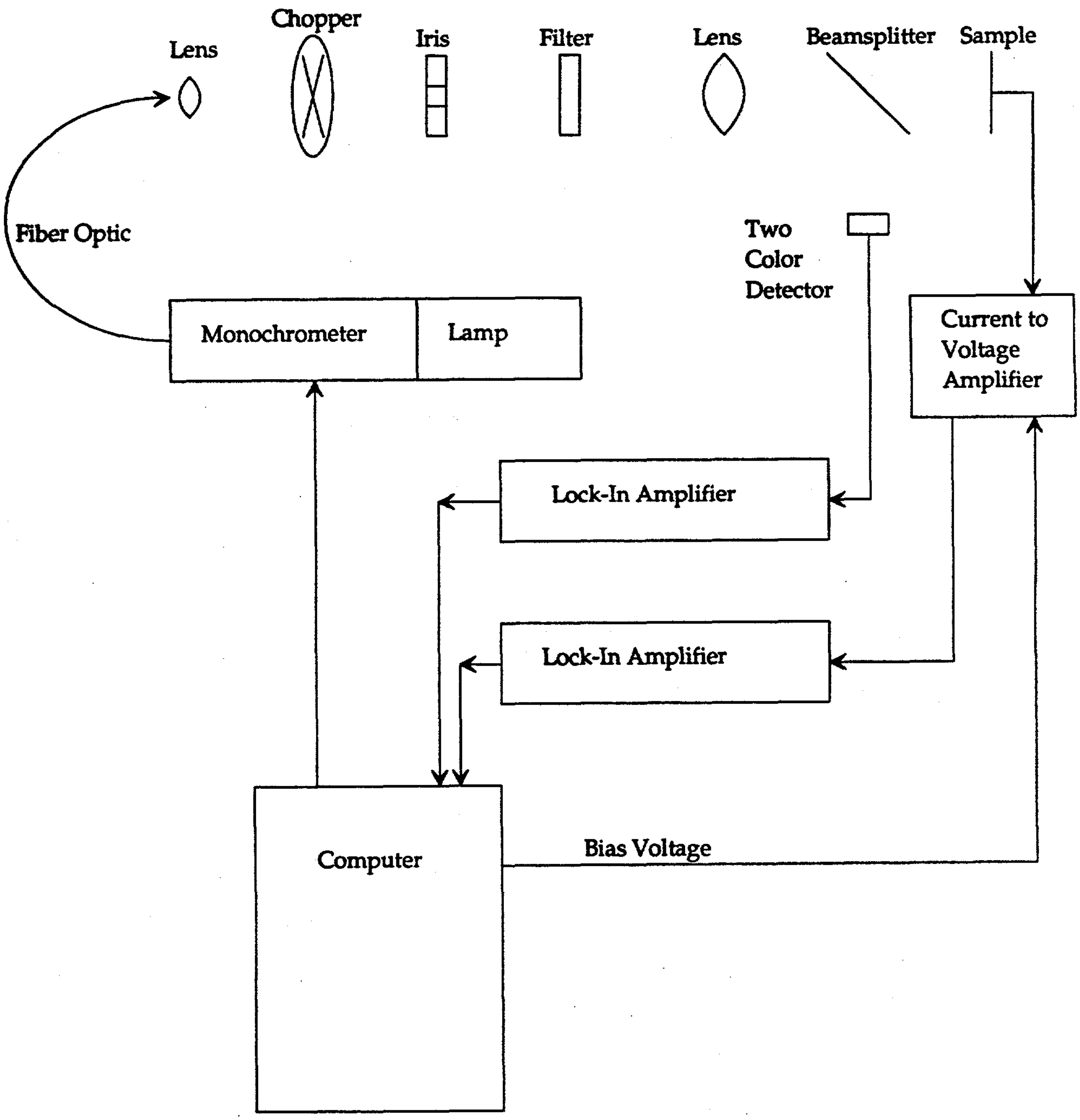

the gratings are changed. The light source is a 12V 50 watt Tungsten-Halogen lamp with a color temperature of 3400°K. Light exiting the monochrometer is collected by a rectangular to circular fiber optic cable. The light is chopped exiting the cable and passed through an iris, then focused on the sample. A piece of Corning 7059 glass is used as a beamsplitter and is placed between the lens and the sample. A detector is placed in the reflected beam's path. This detector is a commercially available "two-color" detector with a silicon germanium photodiode. The output of both photodiodes are wired in parallel and this signal is fed into the current input of a Lock-In Amplifier. The system is capable of measuring the external quantum of a single junction device from 400 nm to 1400 nm, in steps of 20 nm. These measurements can be made both with/without light bias and with/without forward or reverse electrical bias. The system is calibrated with a crystalline silicon-germanium two-color mechanically stacked cell.
The signal from the CIS sample is amplified by a current-to-voltage converter which was built in-house. It will handle high currents when the cell under test is biased at 1 sun intensity. It also has a separate input which allows a bias voltage to be applied to the sample.

Finally, a computer is used to control the measurements, bias voltage, wavelength and calculate the quantum efficiency.

The quantum efficiency measurements under AM1.5 light bias and no electrical bias are integrated with the AM1.5 global spectrum to give the short-circuit current density. A typical output of the measurement is shown in **Figure 4-7** where the upper figure shows the quantum efficiency versus wavelength measurements and the lower figure graphically depicts the optical losses with respect to the AM1.5 global spectrum.

4.3 CIS Device Modeling

The role of the modeling effort in CIS is multi-faceted. First, is to help interpret experimental data seen in developmental solar cells. For this purpose the calculations of the collection efficiency as a function of wavelength, diffusion length, carrier density, grain size, and voltage have been carried out. In addition, the relation of the voltage dependence of the light generated current, to empirically defined series and shunt resistances, has been considered. On a more advanced level are calculations of possible higher efficiency solar cells based upon grading the band edges by use of CuInGaSeS, and CdZnS compounds. These calculations have been primarily analytical.

Figure 4-7. Print-out of typical quantum efficiency of CIS solar cell.

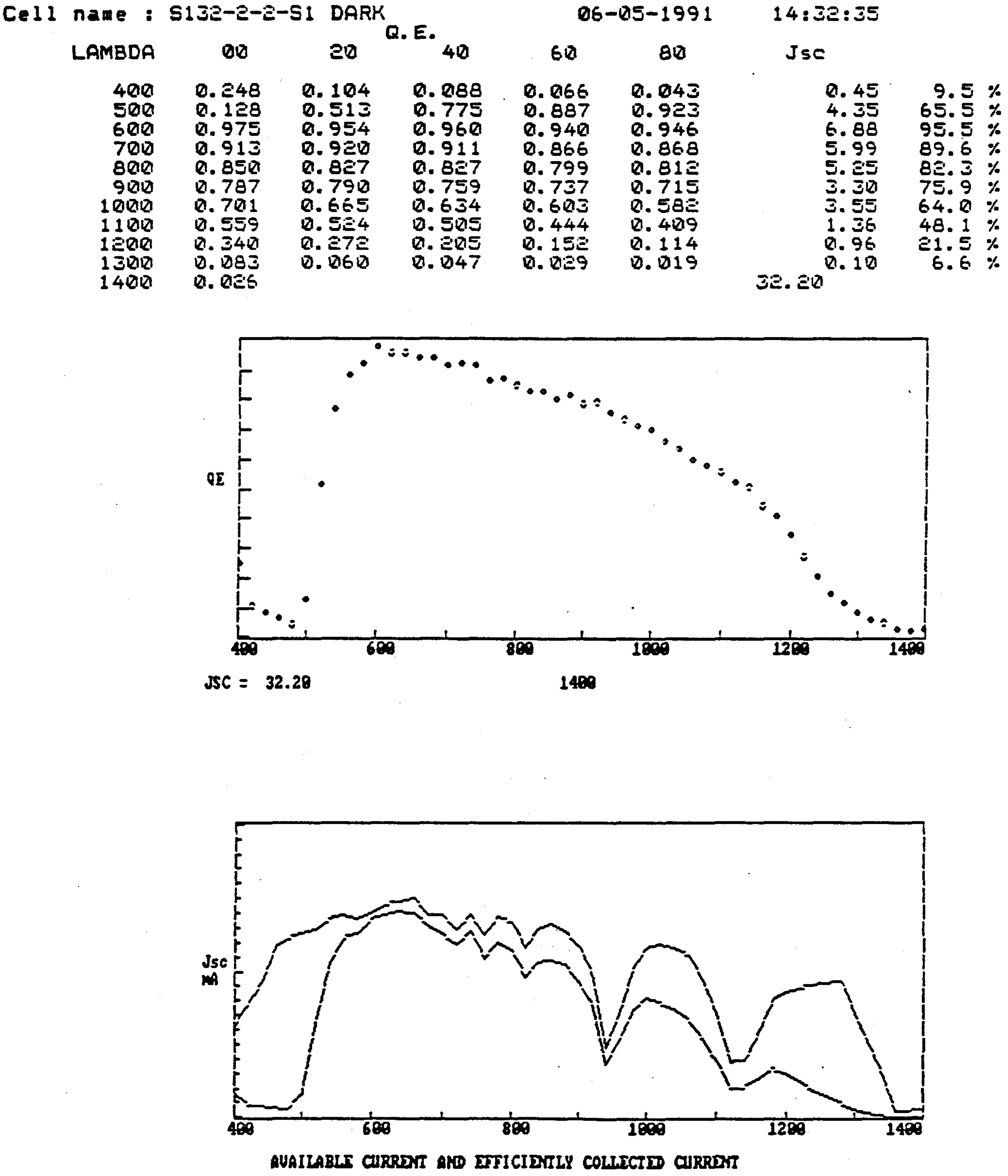

```
Cell name : S132-2-2-S1 DARK                     06-05-1991      14:32:35
                                    Q.E.
     LAMBDA       00        20        40        60        80        Jsc

       400      0.248     0.104     0.088     0.066     0.043              0.45       9.5 %
       500      0.128     0.513     0.775     0.887     0.923              4.35      65.5 %
       600      0.975     0.954     0.960     0.940     0.946              6.88      95.5 %
       700      0.913     0.920     0.911     0.866     0.868              5.99      89.6 %
       800      0.850     0.827     0.827     0.799     0.812              5.25      82.3 %
       900      0.787     0.790     0.759     0.737     0.715              3.30      75.9 %
      1000      0.701     0.665     0.634     0.603     0.582              3.55      64.0 %
      1100      0.559     0.524     0.505     0.444     0.409              1.36      48.1 %
      1200      0.340     0.272     0.205     0.152     0.114              0.96      21.5 %
      1300      0.083     0.060     0.047     0.029     0.019              0.10       6.6 %
      1400      0.026                                              32.20
```

4.3.1 Light Generated Current and Collection Efficiency

The light generated current is the integral over wavelength of the product of the incident flux Φ (λ) and the collection efficiency η $(\lambda.V)$. $\eta(\lambda.V)$ also depends upon the assumed absorption coefficient as a function of wavelength, which also depends upon the composition of the CIS layer. To include grain boundary effects, an analytical expression has been used which calculates the reduction to η (λ) due to the size of the grains, assuming a large value for the grain boundary recombination velocity. The calculated η (λ) as a function of the radius R of the grains and thickness α of the layer has been carried out by simply multiplying the results of the single crystal η (λ, V), by the following factors: For $d < R$, the grain boundary factor is given by

$$\eta_{GB}^{(d<R)} = 1 + \frac{e^{-\alpha d}\frac{d}{R}\left(2 - \frac{2}{\alpha R} - \frac{d}{R}\right)}{1 - e^{\alpha d}} + \frac{2}{\alpha R}\left(\frac{1}{\alpha R} - 1\right) \tag{1}$$

where for $d > R$ the expression is:

$$\eta_{GB}\ (d>R) = \left[1 - \frac{2}{\alpha R} + \frac{2}{\alpha^2 R^2} - \frac{2}{\alpha^2 R^2}\, e^{-\alpha R}\right] / \left(1 - e^{-\alpha d}\right) \tag{2}$$

Using the above expression for the grain size dependence, analytic calculations for the light generated current in the CIS layer as a function of voltage (with doping density and diffusion length as parameters) have been carried out. This involves calculating the current collected in the space charge region as well as that in the neutral region. The collection of electron-hole pairs generated in the space charge region depends upon the applied voltage through two aspects, first the collection depends upon the electric field which changes with applied voltage, second the width of the space charge region changes with voltage. The width of the space charge region depends upon the doping density N_A in the CIS. The effectiveness of the field in collecting the carriers depends upon the electron diffusion length, L, through the parameter of a critical field $Fc = kT/qL$. The collection beyond the space charge region also depends upon L. The consequences of the voltage dependence of the light generated current density L are that the collection efficiency versus wavelength, $\eta(\lambda)$, will be voltage dependent, and there will be a loss in fill factor due to this cause.

Our calculated results show the interplay of N_A and L, $\eta(\lambda,V)$, and the loss in fill factor ΔFF

$$\Delta FF = \left(\frac{J_L\ (0) - J_L(V_{mp})}{J_L(0)}\right) \frac{V_{mp}}{V_{oc}} \tag{3}$$

The value of V_{mp} can be obtained by assuming an expression for the dark diode current and combining it with J_L (V) through the equation $j = j_{diode}$ (V) - j_L (V).

A further consideration is that the effective series resistance as measured from the slope of the I-V curve at V_{oc} can be strongly affected by J_L (V). The apparent shunt resistance is also affected. The expressions for these quantities are:

$$R_s \text{ effective} = (R_s^o + \frac{AkT}{qI_{sc}f(V_{oc})}) / (1 + \frac{AkT}{q} \mid \frac{f'(V_{oc})}{f(V_{oc})} \mid) \tag{4}$$

$$R_s \text{ effective} = R_{sh}^o / (1 + R_{sh}^o I_{sc} f' (V=O) \mid) \tag{5}$$

where J_L (V) = I_{sc} f (V) R_s^o is the true series resistance due to bulk and contact effects, and R_{sh}^o is the true shunt resistance due to leakage paths and A is the diode ideality factor.

One of the purposes of this work is to provide simulations that will allow experimental groups to quickly extract key material and transport properties from collection efficiency measurements. The program calculates the collection efficiency as a function of doping density in the CIS, diffusion length, voltage and grain size. From an SEM of the cell material a grain size is chosen, and the experimental collection efficiency versus wavelength at three voltages is entered. The program then calculates collection efficiencies for a range of diffusion lengths and carrier densities, and compares the experimental and theoretical results, using a least square deviation criteria. The combination of diffusion length and doping density that fits the experimental data best is then displayed with comparison plots of the experimental and simulation results.

Figures 4-8 through **4-14** show the range of variation seen in $\eta(\lambda, V)$ as well as the comparison to experimental results.

4.3.2 <u>Modeling of Graded Bandgap Layers in CIS</u>

The simplest analytic results for graded bandgaps can be obtained by assuming that the grading is linear from front to back (or vice versa) and that the graded region is undoped. Two calculations have been carried out. The first was for a uniform gap with an undoped region of width, w. The second was for a region linearly graded from front to back over a width, w. The first serves as a check on the second, since the second one reduces to the first in the limit δ Eg→0.

Figure 4-8. Quantum efficiency relation showing applied voltage dependence for diffusion length, L = 0.1 μm and Na = $10^{16}/cm^3$ (1. Va = -1V; 2. Va = 0V; 3. Va = 0.3V).

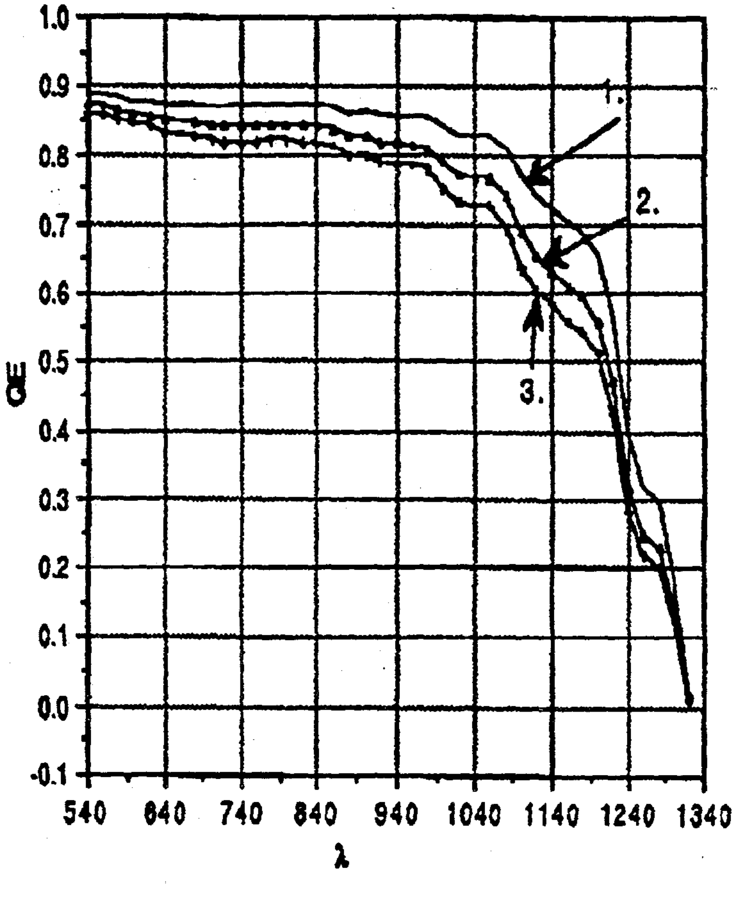

Figure 4-9. Quantum efficiency relation showing concentration dependence for short diffusion length, L = 0.1 μm (1. Na = $10^{15}/cm^3$; 2. Na = $10^{16}/cm^3$; 3. Na = $3.10^{16}/cm^3$).

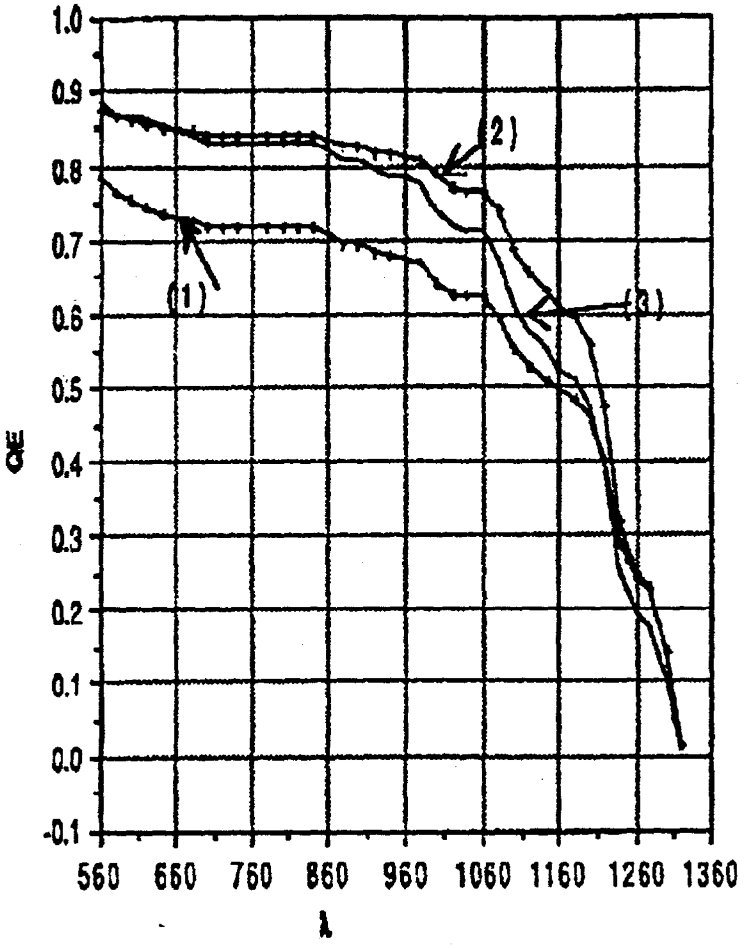

Figure 4-10. Quantum efficiency relation showing grain boundary recombination effect dependence on grain radius for long diffusion length, L = 0.9 μm (1. ideal; 2. R = 0.9 μm; 3. R = 0.5 μm; 4. R = 0.1 μm).

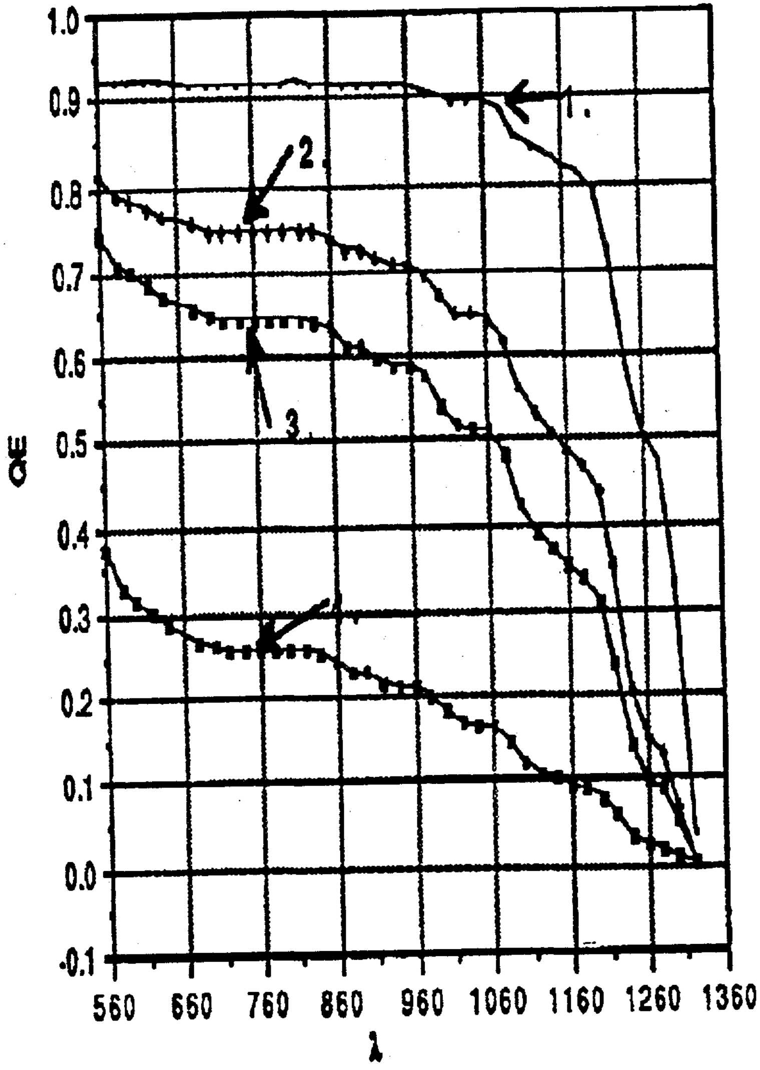

Figure 4-11. Quantum efficiency relation showing minimal concentration dependence for long diffusion length, L = 0.9 μm (1. Na = $10^{15}/cm^3$; 2. Na = $10^{16}/cm^3$; 3. Na = $3.10^{16}/cm^3$.

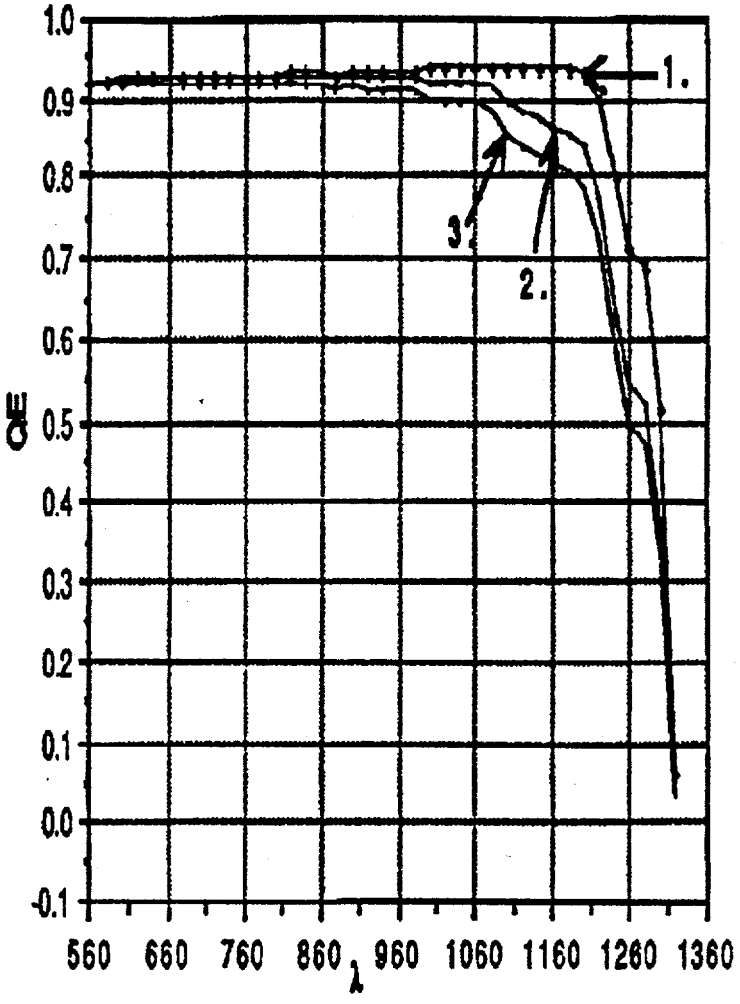

Figure 4-12. Quantum efficiency relation showing diffusion length dependence. (1. L = 0.9 μm; 2. L = 0.5 μm; 3. L = 0.1 μm).

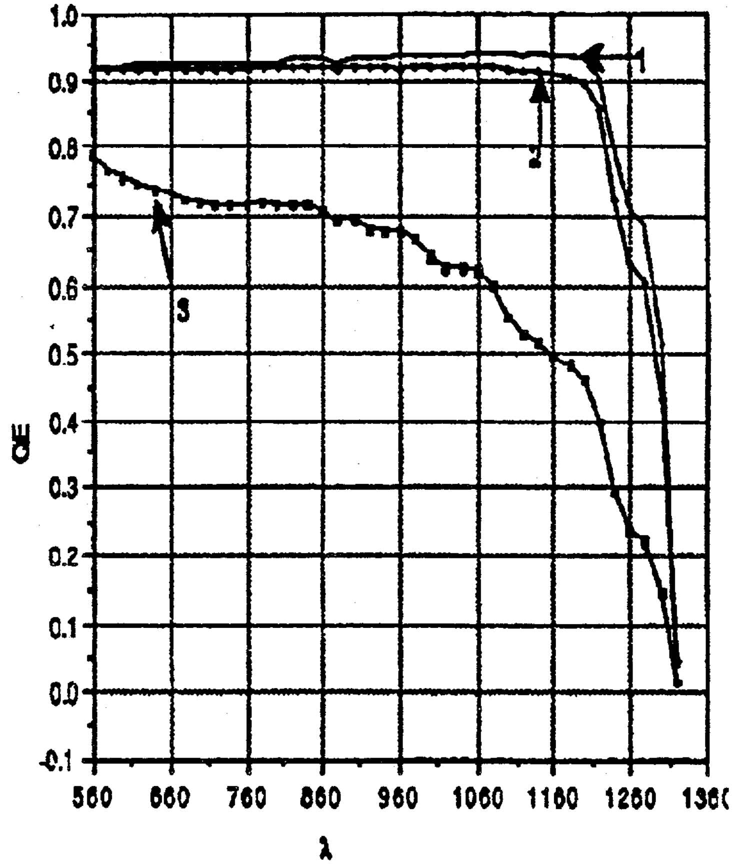

Figure 4-13. Theoretical and experimental efficiencies at Va = 0 for cell S132. SEM grain radius 0.65 μm. Composition: Cu = 19.64%; In = 25.46%; Se = 54.9%. Fitted results Na = $10^{16}/\mathrm{cm}^3$; L = 1.0 μm; J_{sc} = 30.33 $\mathrm{mA/cm}^2$.

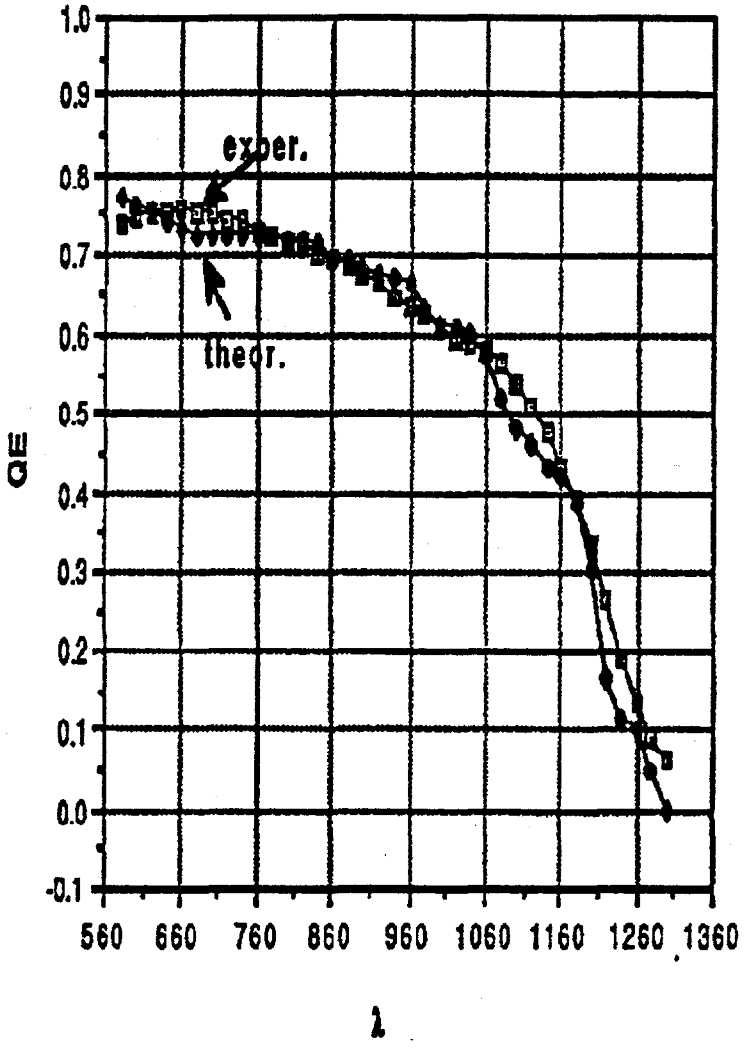

Figure 4-14. Theoretical and experimental efficiencies at Va = 0 for cell S114. SEM grain radius 0.7 μm. Composition: Cu = 24.54%; In = 22.74%; Se = 52.71%. Fitted results Na = $10^{16}/cm^3$; L = 1.0 μm; J_{sc} = 16.03 mA/cm^2.

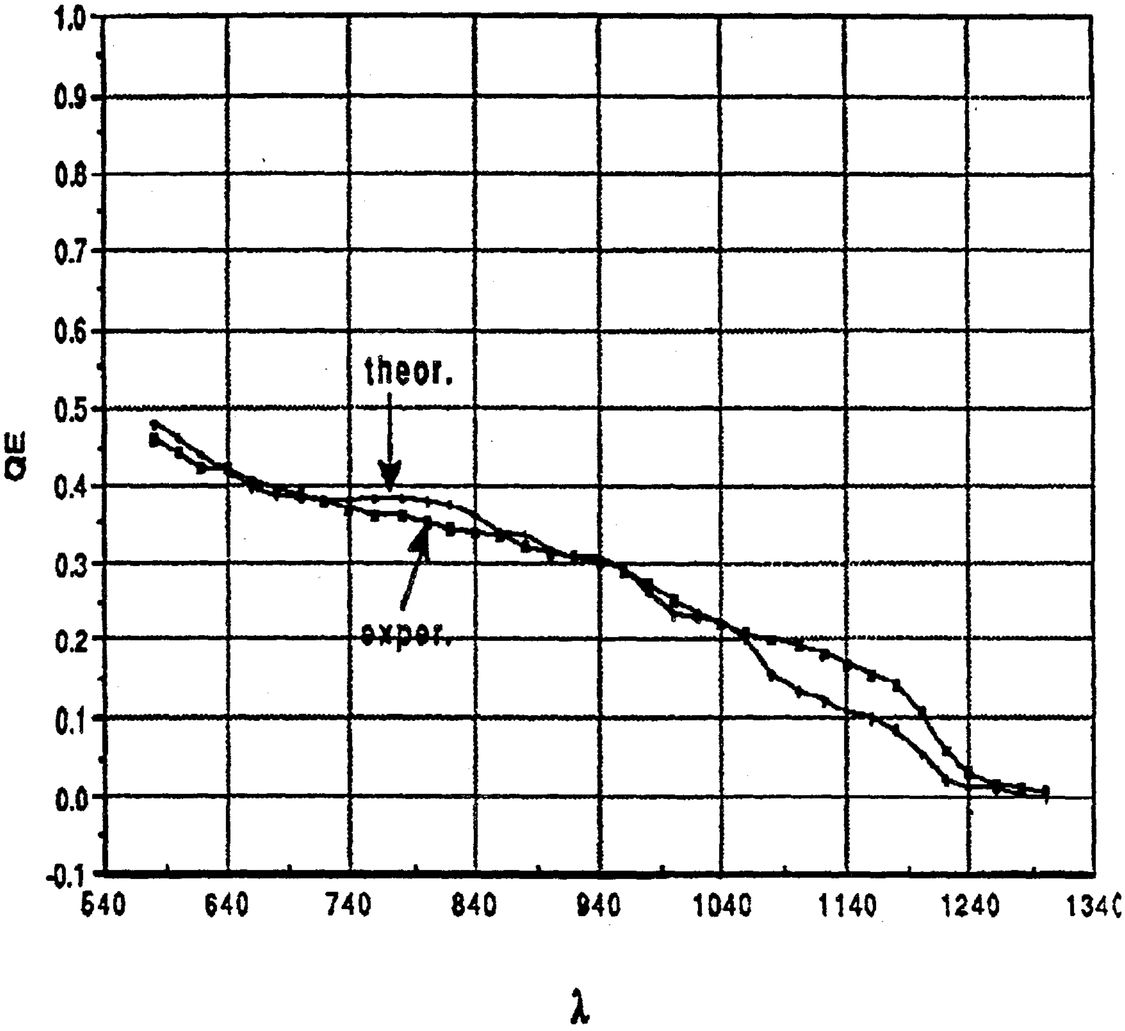

For the ungraded bandgap, the diode current, calculated for recombination by SRH centers at midgap, is given, for lifetime τ, by:

$$j(V_a) = q\frac{n_i w}{\tau}\,\frac{kTe^{qVa/2kT}}{q(V_{bi} - V_a)}\qquad (e\frac{qVa}{kT} - 1)\ \text{arctg}\ (f) \tag{6}$$

where

$$f = (\frac{Nv}{Nc})^{½}\ \frac{e^{-(E_g - 2\delta n - qVa)/2kT}\ (e\frac{q(V_{bi} - V_a)}{kT} - 1)}{1 + \frac{Nv}{Nc}\ e^{(\delta_n - \delta_p)/kT}} \tag{7}$$

and

Va = applied voltage
ni = intrinsic carrier density
V_{bi} = built-in voltage = $(E_g - \delta_n - \delta_p)/q$
$\delta n = E_c - E_F$ in n-material
$\delta p = E_F - E_v$ in p-material
$N_{c(v)}$ = effective density-of-states in conduction (valence) band

Over most of the range arctg (f) = π/2. Only very near flat band as $V_a \rightarrow V_{bi}$ does it come in to cancel the zero in the denominator and the kT in the numerator and give a factor on the order of unity. We note that over the range of interest the diode factor n is equal to 2.

For the graded case the result is similar but the diode factor n is no longer 2, the voltage dependent factor in the denominator is modified and the arctg function is replaced by another related function. The expression is for $V_a < V_{bip}$:

$$j(V_a) = \frac{qn_i(o)\,wkT}{2\tau[q(V_{bip} - V_a) + \delta Eg]}\ e - \frac{\delta E_g}{2kT\,(1 + \frac{\delta E_g}{V_{bip}})}\ e\frac{qV_a}{nkT}\ [B(u) + B(1-u)] \tag{8}$$

where V_{bip} = built-in voltage in valence band = $(E_g\ (o) - \delta_n - \delta_p/q$
$\delta E_g = E_g(w) - E_g(o)$

$$B(u) = \int_0^{\infty} \frac{e^{-uv}}{1 + e^{-v}}\, dv \tag{9}$$

$$u = \frac{q(V_{bip} - V_a) + \delta E_g)}{2(q(V_{bip} - V_a) + \delta E_g/2}$$

$$n = \text{diode factor} = \frac{2(1 + \delta Eg/2V_{bip})}{1 + \delta Eb/V_{bip}}$$

Note that for $\delta E_g = 0$, $n = 2$, $u = 1/2$ and B (u) goes over into arctg. The results indicate that in grading E_g from 1 eV to 1.5 eV a diode factor of $n \sim 1.6$ would occur for $V_a < V_{bip}$, changing to $n = 2$ as $V_a \to V_{bip}$.

Figure 4-15 is a plot of Ln j versus V_a for the analytic case, with the grading indicated. Consideration of the band diagram in equilibrium will reveal that if we grade from the interface into the material, with no offset in the conduction band at the interface, there will be three built-in voltages, V_{bi} in the vacuum level, V_{bin} in the conduction band and V_{bip} in the valence band. V_{bip} and V_{bin} are independent of whether one grades the valence band or the conduction band depending only on E_g, while V_{bi} depends upon which band is graded. Since V_{oc} is limited ultimately by the voltage which brings either of the bands to the flat band condition, for improved V_{oc} not only should grading the band be considered but also shifting the conduction and valence bands at the interface; both the n- and p-material shifts are potentially useful.

Figure 4-15. J(Va) for Eg (0) = 1 eV, Eg (1 μm) - 1.5 eV, $\tau = 10^{-7}$ sec. $J_{sc} = 40$ mA/cm^2, $V_{oc} = 0.63$V.

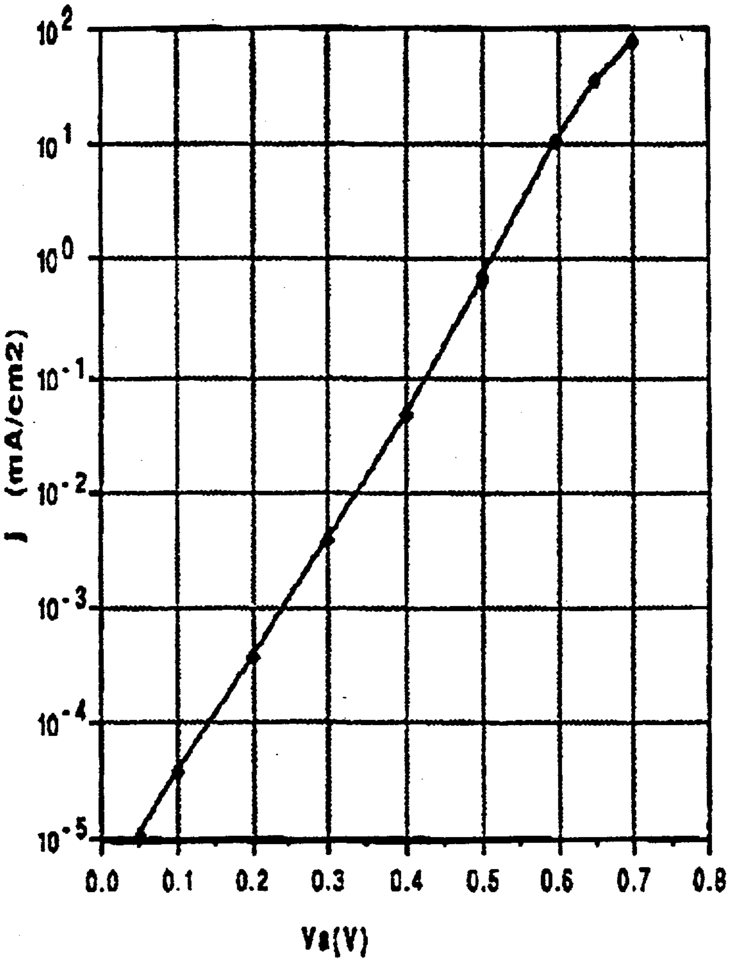

REFERENCES

1. R.R. Potter, C. Eberspacher, L.B. Fabick, Proceedings of the 18th IEEE Photovoltaic Specialists Conference (IEEE, N.Y., 1985), p. 1659.
2. W.E. Devaney, R.A. Mickelson, W.S. Chen, Proceedings of the 18th IEEE Photovoltaic Specialists Conference (IEEE, N.Y., 1985), p. 1733.
3. B. Basol, et al. Proceedings of the 22nd IEEE Photovoltaic Specialists Conference (IEEE, N.Y., 1991), p. 1918.
4. K.W. Mitchell, H.I. Liu, Proceedings of the 20th IEEE Photovoltaic Specialists Conference (IEEE, N.Y., 1988), p. 1461.
5. R.A. Mickelson, B.J. Stansbery, J.E. Avery, W.S. Chen, Proceedings of the 19th IEEE Photovoltaic Specialists Conference (IEEE, N.Y., 1987), p. 744.
6. V.K. Kapur, B. Basol, Tech. Dig. of the PVSEC-5 (1990), p. 751.
7. K. Zwiebel, H.S. Ullal, R.L. Mitchell, Proceedings of the 21st IEEE Photovoltaic Specialists Conference (IEEE, N.Y., 1990), p. 458.

Document Control Page	1. NREL Report No. NREL/TP-413-4906	2. NTIS Accession No. DE92010584	3. Recipient's Accession No.

4. Title and Subtitle

Research on Polycrystalline Thin Film Submodules Based on $CuInSe_2$ Materials

5. Publication Date

May 1992

6.

7. Author(s)

A. Catalano, R. Arya, L. Carr, B. Fieselmann, T. Lommasson, R. Podlesny, L. Russell, S. Skibo, A. Rothwarf, R. Birkmire

8. Performing Organization Rept. No.

9. Performing Organization Name and Address

Solarex Thin Film Division
826 Newtown-Yardley Road
Newtown, PA 18940

10. Project/Task/Work Unit No.

PV231101

11. Contract (C) or Grant (G) No.

(C) ZN-1-19019-4

(G)

12. Sponsoring Organization Name and Address

National Renewable Energy Laboratory
1617 Cole Blvd.
Golden, CO 80401-3393

13. Type of Report & Period Covered

Technical Report
11 November 1990 - 31 October 1991

14.

15. Supplementary Notes

NREL technical monitor: H.S. Ullal

16. Abstract (Limit: 200 words)

This report describes progress during the first year of a three-year research program to develop 12%-efficient $CuInSe_2$ (CIS) submodules with area greater than 900 cm^2. To meet this objective, the program was divided into five tasks: (1) windows, contacts, substrates; (2) absorber material; (3) device structure; (4) submodule design and encapsulation; and (5) process optimization. In the first year of the program, work was concentrated on the first three tasks with an objective to demonstrate a 9%-efficient CIS solar cell.

17. Document Analysis

a. Descriptors

polycrystalline thin films ; submodules ; $CuInSe_2$; photovoltaics ; solar cells ; efficiency

b. Identifiers/Open-Ended Terms

c. UC Categories

273

18. Availability Statement

National Technical Information Service
U.S. Department of Commerce
5285 Port Royal Road
Springfield, VA 22161

19. No. of Pages

76

20. Price

A05

Form No. 0069E (6-30-87)